



**HAL**  
open science

# Impact of Alkyl-Based Side Chains in Conjugated Materials for Bulk Heterojunction Organic Photovoltaic Cells-A Review

Kathleen Isabelle Moineau-Chane Ching

► **To cite this version:**

Kathleen Isabelle Moineau-Chane Ching. Impact of Alkyl-Based Side Chains in Conjugated Materials for Bulk Heterojunction Organic Photovoltaic Cells-A Review. *Energies*, 2023, 16 (18), pp.6639. 10.3390/en16186639 . hal-04209579

**HAL Id: hal-04209579**

**<https://hal.science/hal-04209579>**

Submitted on 18 Sep 2023

**HAL** is a multi-disciplinary open access archive for the deposit and dissemination of scientific research documents, whether they are published or not. The documents may come from teaching and research institutions in France or abroad, or from public or private research centers.


L'archive ouverte pluridisciplinaire **HAL**, est destinée au dépôt et à la diffusion de documents scientifiques de niveau recherche, publiés ou non, émanant des établissements d'enseignement et de recherche français ou étrangers, des laboratoires publics ou privés.



Distributed under a Creative Commons Attribution 4.0 International License

Review

# Impact of Alkyl-Based Side Chains in Conjugated Materials for Bulk Heterojunction Organic Photovoltaic Cells—A Review

Kathleen Isabelle Moineau-Chane Ching <sup>1,2</sup> 

<sup>1</sup> CNRS, LCC (Laboratoire de Chimie de Coordination), 205 route de Narbonne, BP 44099, CEDEX 4, 31077 Toulouse, France; kathleen.chane@lcc-toulouse.fr

<sup>2</sup> LCC-CNRS, Université de Toulouse, CNRS, INPT, UPS, CEDEX 4, 31077 Toulouse, France

**Abstract:** The research for efficient organic materials organized in bulk heterojunction (BHJ) thin films for organic photovoltaics (OPVs) has shown a significant breakthrough in the past decade. Desired structural organization can be attained through various strategies. In this regard, the current review highlights tuning of alkyl chains introduced on molecular structures of active materials. The recent wide literature is classified based on the introduction of alkyl chains on polymers and small molecules used as donor and acceptor materials. The design of these materials, the morphological aspects of the active layers, and the performances of the related photovoltaic cells are detailed. A comprehensive discussion on chemical structures of the different material families considered, their modification by alkyl chains of various natures, and the morphological aspects are reported and tabulated.

**Keywords:** alkyl side chains; organic materials; organic photovoltaics;  $\pi$ -conjugated materials; blend morphology



**Citation:** Moineau-Chane Ching, K.I. Impact of Alkyl-Based Side Chains in Conjugated Materials for Bulk Heterojunction Organic Photovoltaic Cells—A Review. *Energies* **2023**, *16*, 6639. <https://doi.org/10.3390/en16186639>

Academic Editor: Luigi Vesce

Received: 28 July 2023

Revised: 1 September 2023

Accepted: 9 September 2023

Published: 15 September 2023



**Copyright:** © 2023 by the author. Licensee MDPI, Basel, Switzerland. This article is an open access article distributed under the terms and conditions of the Creative Commons Attribution (CC BY) license (<https://creativecommons.org/licenses/by/4.0/>).

## 1. Introduction

Electronic devices are an integral part of everyday life and, among them, solar cells take a growing role. After years of exploration, effective materials for photovoltaics have been developed leading to various technology devices, such as perovskite and quantum dots with the current record efficiency at over 25% [1–5]. Additionally, organic photovoltaics (OPVs) have rapidly become attractive due to their solution-processability, low cost, light weight, flexibility, semi-transparency, and optical tunability advantages. Since the pioneering works of Tang on organic solar cells (OSCs) [6], different concepts have been proposed for OSCs' elaboration [7–9]. The organic photovoltaic effect originates from electronic phenomena resulting from interaction of  $\pi$ -conjugated semiconducting organic materials with solar light. The active layer is classically constituted of two kinds of organic materials, one being the electron donor (D), the other the electron acceptor (A). Among the set-up technologies for active layers, bulk heterojunction (BHJ) solution-processing was described for the first time in 1995 by G. Yu et al. for a polymer/polymer system [10] and then by Peumans and coworkers in 2003 for small-molecule-based thin films [11]. OSCs built from BHJs, in which D and A materials form entangled nanodomains, have been subject to numerous studies for two decades owing to their flexibility and light weight making them attractive for nomad applications associated with potential esthetic features. It is now well established that light conversion into electricity by such cells proceeds according to a series of successive electronic processes: (1) light absorption by the active materials to form excitons; (2) exciton diffusion to D/A interface; (3) exciton dissociation and charge separation at the interface to generate hole and electron charge carriers; (4) hole and electron migration through D and A materials towards the anode and the cathode, respectively; and (5) charge collection at the respective electrodes [12,13]. Each step has been subject to tremendous work in order to improve conversion efficiencies.

The power conversion efficiency (PCE) of OSCs is directly linked to short-circuit current density ( $J_{SC}$ ), open-circuit voltage ( $V_{OC}$ ), and fill factor (FF) [14], those parameters being directly linked to the physicochemical parameters of the active molecules: (i) the D and A materials must exhibit a broad and efficient solar light absorption, favorable for increasing the short-circuit current density ( $J_{SC}$ ) [15,16], (ii) adequate energy levels of their frontier orbitals (HOMO/LUMO) contribute to optimizing the open circuit voltage ( $V_{OC}$ ) [17–19], (iii) when optimized relatively to the Fermi levels of the electrodes, these energy levels also favor electron and hole transport efficiency to the electrodes [20–24], (iv) and ordered  $\pi$ - $\pi$  packing of D and A aggregates in optimized BHJ morphology, high domain purity, and symmetric carrier transport in the blend contribute to high FF [17,25,26]. As examples of recent improvements leading to record efficiencies, interlayer engineering as well as n-doping are strategies that have been successfully employed: BHJ OSCs have reached interesting record PCEs of 17% in 2019 via optimization of the hole-transporting layer (HTL) used as interfacial anode material [27] and of 17.1% in 2020 via the use of n-type dopant [28]. During the same period, an equivalent record PCE of 17% was reached via optimization of chemical structures of active materials, demonstrating the decisive role of synthetic chemistry [29]. In particular, the design strategy of non-fullerene acceptors (NFAs) has recently led to an impressive improvement in the performance of OSCs, these materials offering broad absorption spectra, tunable energy frontier levels, various modes of molecular packing, and optimized phase-separation morphologies [7,30]. Many works are currently still devoted to the optimization of molecular structures of polymers and/or small molecules, the preparation process, the design and optimization of interface materials, the use of additives, and the device engineering, as attested by recent reviews summarizing the remarkable improvements achieved in recent years in terms of efficiency, with PCE values up to 20% [31–33]. In terms of molecular engineering, and besides the molecular structures themselves, one of the crucial aspects of OPV engineering has been revealed to be the control of the packing capacity of organic materials. As an example, Wang et al. proposed to use aggregation-induced emission (AIE) properties of tetraphenylethylene (TPE) derivatives in order to improve interfacial cathode materials' performance and obtained a 2.3 times increase in PCE [34]. Likewise, the control of molecular packing of organic materials constituting the BHJ is better and better anticipated thanks to optimization of  $\pi$ -conjugated molecular structures and alkyl side chains, as was carried out for liquid crystal self-assemblies [35]. The well-known case of poly-3-hexylthiophene (P3HT) is a typical and pioneering example: the control of P3HT regiochemistry aiming at obtaining highly regioregular head to tail (RR-HT) polymer was first achieved from 1992–1993 by McCullough [36,37] and Rieke [38]. The hexyl chains rapidly proved to favor the structural order in RR-HT polythiophene, leading to remarkable charge mobilities [39]. P3HT was established in the early 2000s as a promising D polymer for OPV [40,41] alternatively to poly-(para-phenylene-vinylene) (PPV), one of the most thoroughly investigated so far. Since this time, synthetic methodologies have been developed to obtain in high yields RR-HT P3HT with controlled molecular weight ( $M_n$ ) and/or polydispersity index (PDI), leading to P3HT polymers with attractive structural, electronic, and optical properties, as demonstrated in recent research papers [42–45] and reviews [46–49]. With this review, we will focus, from a chemist point of view, first on polymer-based systems, then on small-molecule-based systems, with particular attention to the nature (linear or branched), length, and branching position of alkyl chains on the molecular backbones of A-D-A materials used in OPVs. Here, "A" and "D" represent the electron-withdrawing and electron-donating moieties, respectively, in the active small molecule or polymer.

Alkyl chains were first used to circumvent solubility issues in usual organic solvents and allow solution-processable processes for elaboration of organic electronic devices. During the last decade, there has been a growing interest in side chain engineering for improving thin film morphology and charge mobility in polymers [50] and in organic materials in general [51,52]. This demonstrates the interest in introducing suitable alkyl chains on promising  $\pi$ -conjugated systems to successfully combine the material organi-

zation and electronic properties. In this review, recent examples of successful alkyl chain engineering will be reported, demonstrating that not only can the optoelectronic properties of each organic component, polymer, or small molecule be improved in bulk but also that a synergic effect between D and A materials can be fruitfully reached in blends used for OPV systems through alkyl side chain engineering.

## 2. Polymer-Based Systems

Since the first use of conjugated polymers in organic electronics [53], research on their design has led to impressive progress of OPV performances. Numerous hundreds of publications have reported the synthesis, photophysical properties, and use of conjugated polymers in OPVs. Several reviews have gathered these papers [54–56], emphasizing the polymerization strategy [57], the role of specific building blocks [58–61], the improvement of the active layer or cell technology [9,62,63], the achievement of transparent BHJ photoactive layers and devices [54,64], or their morphological design strategies for improving charge carrier mobilities [65]. Recently, conjugated polymer-based bulk heterojunction solar cells have exhibited high power conversion efficiencies (PCEs) up to 18.22% in 2020 [66] and up to 19.3% in a single-junction cell in 2022 [67]. The role of side chain engineering in solution-processable conjugated polymers is taking a growing role in these record performances. The side chains may be of various chemical types, namely, alkyl, hybrid, oligoether, fluoroalkyl, and latently reactive side chains, as detailed in the first review devoted to side chain engineering for polymer-based solar cells [50]. Here, we will focus on the three first classes, as we do not intend to give an exhaustive coverage of the topic but highlight the most representative examples. The structures of the polymers that are subjects of this review are represented in Figure 1. The n-type organic semiconductors evoked in this part are represented in Figure 2.

It has been very recently pointed out that in polymer systems, one of the main challenges is to obtain efficient and stable BHJ morphological states as soon as the thin film is elaborated, both at the laboratory scale in using spin coating techniques and on an industrial scale where printing methods are preferred [68]. In the first case, the deposition of an already prepared blend of donor and acceptor materials affords a BHJ in which an ideal compromise between D/A miscibility and phase separation is required for nanofibrillar structures [67,69]. In the second case, a two-step sequential deposition method proved to favor the formation of fibril structure of donor polymer in the first layer in which NFA molecules can diffuse into the fibril mesh to form a bicontinuous network morphology [68]. A low miscibility of both materials is detrimental to morphology stability and may be responsible for spontaneous spinodal D/A demixing, as a major issue in BHJ morphology degradation [70]. For investigating blends' morphology, spectroscopic means such as UV–visible (UV–Vis) spectroscopy are commonly used on solutions and thin films, as well as high-resolution techniques: while the polymer packing behavior may be investigated by grazing-incidence wide-angle X-ray scattering (GIWAXS), that has emerged as a powerful tool in the past two decades for the study of nanostructuration in thin films, atomic force microscopy (AFM) and transmission electron microscopy (TEM) are also used for analyzing the impact of morphology on  $J_{SC}$  and FF.

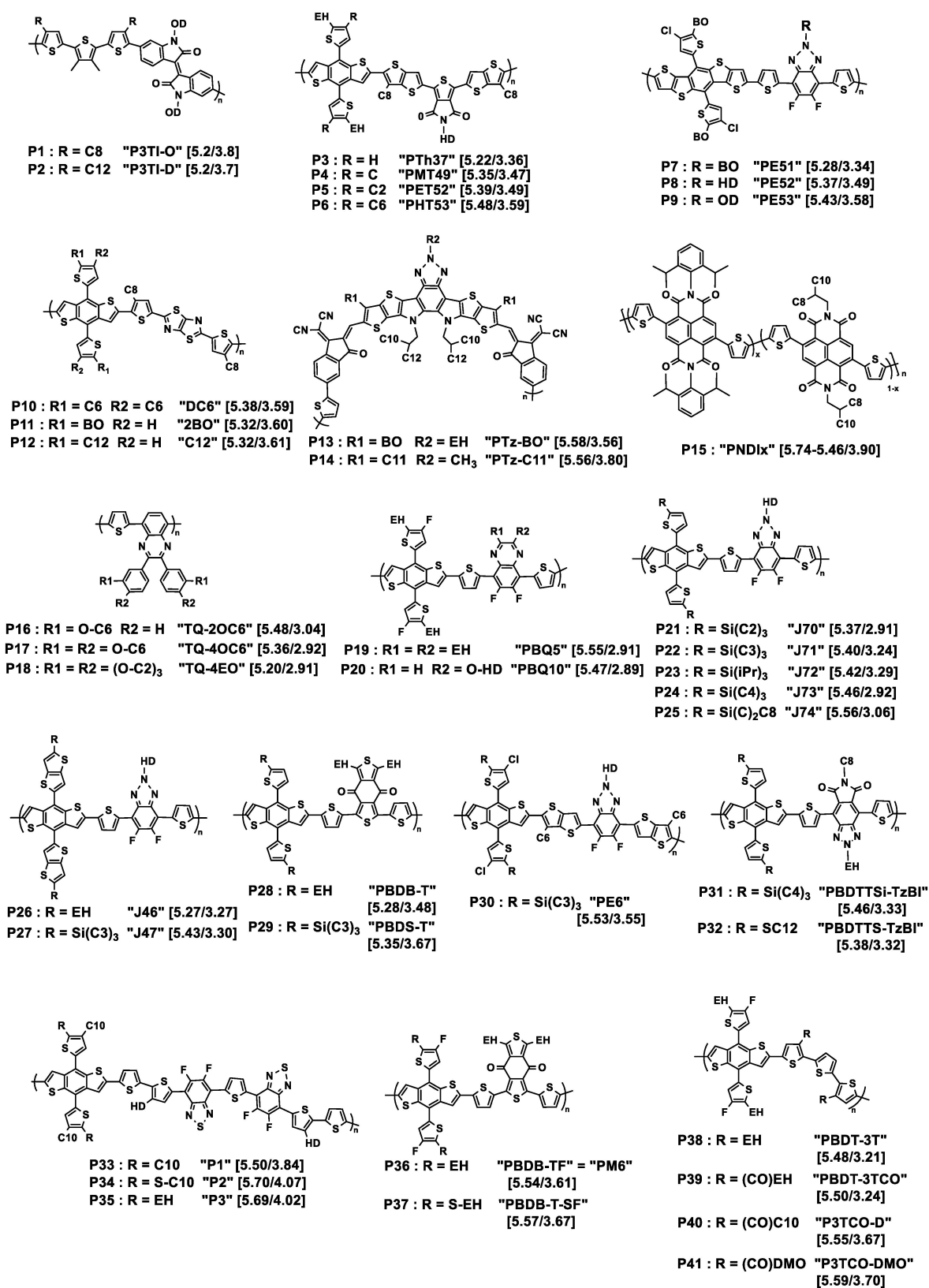


**Figure 1.** Chemical structures of the donor polymers discussed in this review. Px is the abbreviated name of the polymer whose original name is also given in quotation marks. HOMO/LUMO energy levels (eV) are given in square brackets. EH = 2-ethylhexyl; BO = 2-butyloctyl; HD = 2-hexyldecyl; OD = 2-octyldodecyl; DMO = 3,7-dimethyloctyl; iPr = isopropyl. Cx = *n*-alkyl linear chain with *x* methylene units.

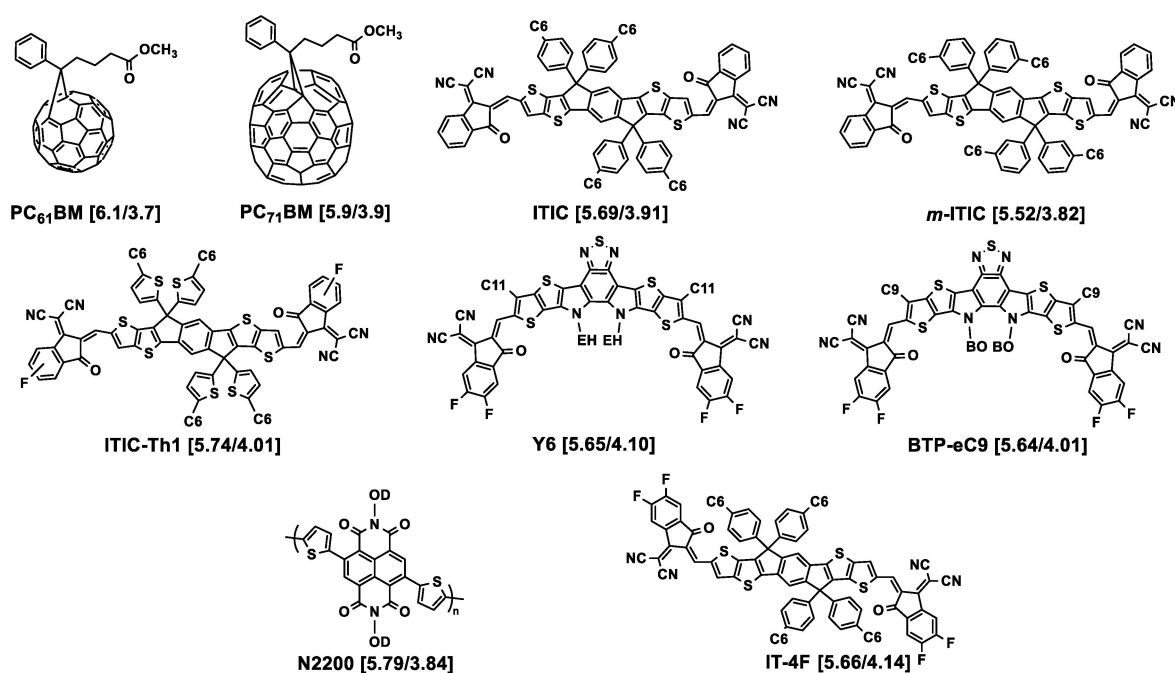


**Figure 2.** Chemical structures of the acceptors used in association with the polymers described in this section. HOMO/LUMO energy levels (eV) are given in square brackets. EH = 2-ethylhexyl; BO = 2-butyloctyl; OD = 2-octyldodecyl. Cx = *n*-alkyl linear chain with x methylene units.

### 2.1. Length of *n*-Alkyl Chains

- Tegene and collaborators have prepared two polymers based on terthiophene-isoindigo bricks [71]. While the indigo unit is functionalized on the N atoms by bulky 2-octyldodecyl branched chains, the authors have grafted *n*-alkyl chains of two different lengths onto the terthiophene unit, a C8 and a C12 chain (see **P1**, **P2** in Figure 1), in order to probe the effect of their length on the early photoinduced charge-transfer process. Whereas the chain length had a negligible effect on absorption and emission (steady-state measurements) in solution and thin films, femtosecond transient absorption (fs-TA) spectroscopy revealed that the intramolecular charge-transfer process was three times faster in going from a C12 to a C8 chain. Moreover, exciton–exciton annihilation (EEA) measurements together with estimation of exciton density demonstrated that the exciton diffusion was boosted when the alkyl side chain was shorter. The authors suggested that these results were related to better intra- and interchain interaction in the polymer with shorter alkyl chains. The model case with no alkyl chain on the terthiophene moiety was not reported.
- Playing with shorter chains, Zhang and collaborators explored the effect of length of linear alkyl chains from C1 to C6 in the 4-position of the pendant thiophene moiety of the 4,8-di(thien-2-yl)benzo [1,2-*b*:4,5-*b'*]dithiophene (DTBDT) unit, including the case of no chain being grafted, of polymers resulting from the polycondensation of the benzo [1,2-*b*:4,5-*b'*]dithiophene (BDT)-based monomers with 5-(2-ethylhexyl)-1,3-bis(3-octylthieno [3,2-*b*]thiophen-5-yl)-5*H*-thieno [3,4-*c*]pyrrole-4,6-dione (tt-TPD) monomers [72]. The structures of the corresponding polymers **P3** to **P6** are shown in Figure 1. While they named the polymer without grafted alkyl chain PTh37, PMT49, PET52, and PHT53 were those with methyl, ethyl, and *n*-hexyl chains on the 4-position of the pendant thiophene moiety, respectively. All the polymers are substituted in the 5-position by an ethylhexyl branched chain, thus situated in the vicinity of the linear chain. It was observed by UV–Vis spectroscopy that the optical bandgaps were 1.86, 1.88, 1.90, and 1.89 eV for PTh37, PMT49, PET52, and PHT53, respectively, demonstrating low impact of the alkyl chains. However, comparison of the thin film spectra revealed a stronger vibrational character of the 500 to 640 nm absorption band

with increasing the length of the alkyl chain, suggesting enhanced intermolecular interactions with alkyl chain growth. The photovoltaic parameters of devices prepared with ITIC as the acceptor demonstrated that the methylated polymer PMT49 afforded the best performances, delivering a PCE of 12.1%, against 10.9%, 9.94%, and 8.05% for devices based on PTh37, PET52, and PHT53, respectively. The  $J_{SC}$  values evolved in the same way, from 18.52 mA cm<sup>-2</sup> for PMT49:ITIC to 17.63 mA cm<sup>-2</sup>, 15.74 mA cm<sup>-2</sup>, and 13.69 mA cm<sup>-2</sup> for PTh37:ITIC, PET52:ITIC and PHT53:ITIC, respectively. Studies performed on thin pristine films and their blends with ITIC confirmed the advantage of PMT49 over the other polymers with higher charge mobilities in blend films and more optimized morphology with smaller domain size (13.09 nm vs. 16.68 nm, 14.67 nm, and 17.38 nm for PTh37:ITIC, PET52:ITIC, and PHT53:ITIC blends, respectively). In that case, it is noticeable that, even with an ethylhexyl branched chain in the 5-position, methyl short chains can finely tune the device performances by exerting a significant influence on the morphology of the resulting polymer and its blends with the acceptor material. Here again, using shorter chains was proved to be beneficial.

## 2.2. Length and Linear/Branched Nature of Alkyl Chains

As seen before, there is a compromise in polymer systems between strong self-aggregation phenomena resulting from  $\pi$ - $\pi$  stacking of the conjugated backbone and reduction of aggregation tendency by using bulky side chains. If we push too far to extremes, in the first case large aggregated domains appear in the film which reduces the polymer miscibility with acceptor materials and, in the second case, the propensity to self-aggregate becomes so weak that the crystallinity of the polymer vanishes, these two cases being causes of phase separation between donor and acceptor [73]. BHJ morphology is linked both to the chemical nature of the donor and acceptor conjugated units forming the polymer backbone and to the substitution sites, the length, or the branching position of the solubilizing side chains. It is often observed that branched alkyl chains positively affect the morphology of thin film in comparison to their linear counterparts, due to their double effect of solubilization and aggregation hindering related to their bulkiness. Tuning this last parameter may influence the way of stacking of conjugated polymer and thus the device performances. A convenient means for this is changing the length of the alkyl chains before and/or after the branching point as reported in several papers.

- Zhou and coworkers prepared three polymers named as PE51, PE52, and PE53 possessing the same polymer backbone but branched alkyl chains of increasing bulkiness from PE51 to PE53, as presented in Figure 1 (polymers P7–P9) [74]. The backbone is constituted by alternating donor DTBDT and acceptor benzotriazole (BTA) moieties, the latter being substituted on the triazole ring by branched alkyl chains, namely 2-butyloctyl, 2-hexyldecyl, and 2-octyldecyl. UV–Vis absorption spectra show that, besides the classical charge-transfer transition absorption peak, the three polymers exhibit vibrational absorption peaks in solution, which is related to intramolecular aggregation. After mixing them with Y6 as the acceptor, the resulting films' parameters were analyzed. It was observed that the  $V_{OC}$  value slightly increases with the bulkiness of the side chains: the PE51, PE52, and PE53 polymers containing 2-butyloctyl, 2-hexyldecyl, and 2-octyldecyl chains, respectively, exhibited  $V_{OC}$  values of 0.79, 0.80, and 0.83 V, respectively. The authors attributed these differences to the changes in HOMO levels induced by the side chains. The trend was different if considering the molecular packing behavior investigated by GIWAXS: while PE51:Y6 and PE52:Y6 blend films exhibited an obvious (010) peak in the out-of-plane (OOP) direction, revealing a face-on orientation, the disappearance of this peak for PE53:Y6 blend film indicated that the polymer with the bulkiest side chains tends to stack out of the film plane. The calculated  $\pi$ - $\pi$  stacking spacing for PE51:Y6, PE52:Y6, and PE53:Y6 (3.58, 3.48, and 3.73, respectively) and crystal coherence length (CCL) (25.41, 28.71, and 12.4 Å, respectively) indicated a strongest stacking, shortest charge-transport distance, and highest crystallinity for the PE52:Y6 blend. Consistently, it achieved

- the best  $J_{SC}$  ( $25.36 \text{ mA cm}^{-2}$ ) and FF (71.94%) values and reached the highest PCE of 14.61% among the examined series. These results were consistent with AFM and TEM analyses which revealed for the PE52:Y6 blend film an increased crystallization tendency of copolymer grains and the best quality of the bicontinuous interpenetrating network. Here, the best polymer is that with intermediate length of branched chains.
- While the preceding examples relate to studies on polymer–small molecules systems, the next three deal with recent studies on all-polymer OPV cells. In the first case, three different D polymers **P10** to **P12** were investigated, with backbones all composed of alternating DTBDT, *n*-octyl-substituted thiophene, and thiazolothiazole (TTz) fragments (see Figure 1) [75]. The only difference between them was the nature of the alkyl chain introduced onto the pendant thiophene rings of the DTBDT fragment. The total number of carbon atoms introduced onto each thiophene ring was always the same, but the nature and number of chains differed from one polymer to another: two *n*-hexyl linear chains for DC6, one 2-butyloctyl branched chain for 2BO, and one *n*-dodecyl linear chain for C12. Absorption spectroscopy performed on thin films revealed no radical difference between them, which was not the case in chlorobenzene solutions in which DC6 showed a strong ability to form  $\pi$ -aggregates with increasing temperature unlike to the two other polymers. Optimized blends and solar cells have been developed using N2200 as the acceptor polymer. Their photovoltaic parameters revealed a clear difference between DC6, for which a PCE of 8.3% was obtained with a  $V_{OC}$  of 0.87 V,  $J_{SC}$  of  $14.2 \text{ mA}\cdot\text{cm}^{-2}$ , and FF of 66.4%, and the two other polymers for which the PCE value did not exceed 2.4%, due to low  $V_{OC}$  and  $J_{SC}$  values. These findings were explained by GIWAXS measurement which demonstrated weak face-on orientation of the backbone for 2BO and C12 while DC6 formed a highly ordered and strong face-on backbone stacking. Measurements of photocurrent vs. the applied voltage confirmed that DC6-based solar cells achieved the highest rate of exciton generation, and the dependencies of  $J_{SC}$  and  $V_{OC}$  on incident light intensity revealed negligible bimolecular recombination for DC6 containing two *n*-hexyl pendant chains per DTBDT unit unlike the other two polymers holding only one bulky linear or branched alkyl chain. Two hexyl chains were revealed to be the best option in that case.
  - In the next example, the effect of the alkyl chains was examined in an acceptor polymer, whose monomer unit was based on a seven-fused-ring system with a central benzotriazole core (see Figure 1, **P13**, **P14**) [76]. Butyloctyl or *n*-undecyl chains were introduced onto the polymer backbone whereas the N atom of the benzotriazole was substituted either by ethylhexyl or by a methyl group. Interestingly, the polymer with butyloctyl/ethylhexyl chains, PTz-BO, exhibited a higher absorption coefficient in solution but a narrower absorption range in thin film than that with *n*-undecyl/methyl chains, PTz-C11. After blending with PBDB-T as the donor polymer, the average electron/hole mobilities of PBDB-T:PTz-BO and PBDB-T:PTz-C11 were  $3.34 \times 10^{-4}/2.26 \times 10^{-4}$  and  $3.71 \times 10^{-4}/2.22 \times 10^{-4} \text{ cm}^2 \text{ V}^{-1} \text{ s}^{-1}$ , with a slightly better  $\mu_e/\mu_h$  ratio for PBDB-T:PTz-BO. The PTz-BO-based device yielded better  $V_{OC}$  and PCE values of 0.928 V and 15.76%, respectively, compared to the PTz-C11-based device (0.882 V and 15.59%), demonstrating a slightly positive effect of branched chains.
  - The third case is about an alternative method to tune the aggregation of alkylated polymer: random copolymerization. This was proposed by taking a naphthalene diimide (NDI)-based series of acceptor polymers (see Figure 1, **P15**) [73]. Random copolymerization between three monomers, namely 2,2'-bithiophene, and two 2,6-dibromonaphthalene-1,4,5,8-tetracarboxylic-diimide units substituted on their N,N'-position by either 2,6-diisopropyl-phenyl or 2-octyldodecyl fragments, respectively, afforded a series of acceptor materials with increasing ratio of aromatic side chain to branched alkyl chain ( $x = 0-1$ ). After blending with the PBDB-T donor polymer, the nine all-polymer BHJs were submitted to morphology and photovoltaic characterization that emphasized the correlation of the optimal obtained PCE of 6.95% obtained



by as-cast blends for  $x = 0.5$  (vs. 5.11% and 1.06% for  $x = 0$  and 1, respectively) with optimal active layer film morphology.

### 2.3. Ethoxy Chains

- Another way to explore the effect of bulkiness of side chains was to use *n*-hexyloxy (C6) and oligoether (tri(ethyleneoxy) (EO)) chains grafted on the meta only or on the meta- and para-positions of the peripheral phenyl ring of the quinoxaline moiety in thiophene–quinoxaline copolymers (see **P16–P18** in Figure 1) [77]. The absorption spectra of the copolymers with meta-para-disubstitution on the phenyl rings (TQ-4OC6 and TQ-4EO) are blue shifted in comparison with that of the meta-substituted copolymer (TQ-2OC6). This was attributed to smaller effective conjugation lengths, as suggested by density functional theory (DFT) results: the calculations highlighted the formation of oligomer chains in a circular-type configuration in the case of meta-para-disubstitution, producing more or less extended chains, which is unfavorable to the formation of polymers of long conjugation length. Consequently, only modest OPV parameters were obtained after blending with PC<sub>61</sub>BM, with PCEs not exceeding 1.27% for the meta-para-disubstituted species and 5.70% for the meta-monosubstituted one, after blending with PC<sub>61</sub>BM as the acceptor. This was surprising owing to PCE of 7% previously obtained with an analogous TQ blended with PC<sub>71</sub>BM and containing an *n*-octyl chain in the meta-position of the phenyl rings [78]. This may be related to the nature of the acceptor, although the deviation of the OPV parameters measured from one laboratory to another cannot be excluded.
- The following example demonstrates the possible positive effect of ethoxy chain: two studies on copolymers based on fluorinated DTBDT and quinoxaline units (see **P19, P20**, Figure 1) were carried out [79,80]. The quinoxaline unit was dialkyl-substituted in PBQ5 and monoalkoxy-substituted in PBQ10. In the two cases, blends with Y6 as the acceptor were elaborated. The best photovoltaic results obtained with PBQ10 (PCE of 16.34% vs. 15.55% for PBQ5) cannot be related to difference in energy offset of the donor/acceptor as the two polymers presented similar HOMO/LUMO energy levels. Hole mobilities, measured by the SCLC method, were of  $2.2 \times 10^{-4}$  and  $5.22 \times 10^{-4} \text{ cm}^2 \text{ V}^{-1} \text{ s}^{-1}$  for PBQ5 and PBQ10, respectively. For the PBQ5:Y6 blend film, the  $\mu_h/\mu_e$  ratio was 0.86. No number was reported for PBQ10:Y6 films. Owing to GIWAXS results, both neat polymer films showed preferential face-on molecular orientation with well-defined  $\pi$ – $\pi$  stacking diffraction peaks ((010) peak) in the out-of-plane (OOP) direction. Well-defined diffraction peaks indicated  $\pi$ – $\pi$  stacking distance of 3.72 and 3.68 Å for PBQ5 and PBQ10, respectively. Contrarily to PBQ5, PBQ10 also exhibited a lamellar distance of 21.12 Å in the OOP direction and a CCL of 27.1 Å, indicating a better molecular self-assembly. In this example, the use of a single branched substituent in the alkoxy form is preferable to that of two ethylhexyl substituents.

### 2.4. Alkylsilyl Chains

Since its first report in 2008 [81], the BDT unit has often been used as a donor unit for polymer elaboration; in particular, it gave rise to its derivative, DTBDT, well known as a donor moiety in A-D-A materials. Similar donor building blocks are widely used because their symmetrical chemical structures and rigid fused aromatic systems benefit the electron delocalization and  $\pi$ – $\pi$  stacking [57] and contributed until very recently to the achievement of outstanding OPV device performances [82]. The DTBDT moiety is built from the commercially available benzo [1,2-*b*:4,5-*b'*]dithiophene-4,8-dione and offers the possibility of introducing a large variety of side chains on the pendant thiophene units. In particular, it has contributed to the generation of PBDB-T-based polymers (see **P36**, Figure 1), a significant milestone in OPVs, which afforded PCEs up to 11.14% in 2019 for a large-scale blade coated binary system [83] and up to 15.83% in 2022 at the laboratory

scale [84]. Some specific DTBDT-based polymers (P21 to P32), designed for investigating the effect of bulky silyl groups, will be discussed hereafter.

- In 2018, Bin and collaborators examined in a systematic manner ((DTBDT/benzotriazole)-based copolymers (see Figure 1, P21–P25) [85]. This polymer series was synthesized for investigating the length and linear or branched character of the alkyl substituents of alkylsilyl side chains of the DTBDT moiety. The optical gaps of the five polymers in thin films were very similar, from 1.96 to 1.99 eV. However, the electrochemical gap changed from 2.13 eV (J72) to 2.50 eV (J74), due to a slightly higher oxidation potential when the bulkiness increased from J70 to J74 together with slightly different values of reduction potential: J70 and J73 were reduced at about  $-1.45$  V/Ag/AgCl, J71 and J72 at about  $-1.10$  V/Ag/AgCl, with J74 being in between. GIWAXS analysis showed that the polymers in neat films are predominantly face-on oriented. The out-of-plane (OOP)  $\pi$ - $\pi$  stacking distance gradually increased from 3.735 Å for J70, to 3.778 Å for J71, 3.792 Å for J72, 3.859 Å for J73, and 3.862 Å for J74, resulting from the effect of bulkiness of the alkylsilyl side chains. Despite modest electron and hole mobility values (below  $10^{-3}$  cm<sup>2</sup> V<sup>-1</sup> s<sup>-1</sup>), good photovoltaic performances were obtained from solar cells with *m*-ITIC as the acceptor, exhibiting PCEs ranging from 9.63% (J74, the polymer with the longer chains) to 12.05% and 11.62% (for J71 and J70, respectively, the polymers with the shorter chains).
- At the same time, the J47 polymer was engineered on the basis of the structure of J71 but with pendant thienothiophenyl fragments attached to the benzodithiophene moiety as an alternative to the thienyl ones (see Figure 1, P27) [86]. This polymer was compared to J46 presenting ethylhexyl instead of tripropylsilyl substituents (see Figure 1, P26). The photovoltaic performances of solar cells elaborated with (3,9-bis(2methylene-(3-(1,1-dicyanomethylene)indanone))-5,5,11,11-tetrakis(4-*n*-hexylphenyl)-dithieno [2,3*d*:2',3'*d'*]-s-indaceno [1,2*b*:5,6*b'*]dithiophene) (ITIC) as the acceptor displayed a maximum PCE of 2.3% for the J46-based system and 7.4% for the J47-based solar cell. This difference was related to the  $J_{SC}$  values that were two times lower for J46 (7.39 mA cm<sup>-2</sup> vs. 16.22 mA cm<sup>-2</sup> for J47) explained by the authors by the low hole mobility and unbalanced charge carrier mobilities in the J46:ITIC blend ( $\mu_h = 0.40 \times 10^{-5}$  cm<sup>2</sup> V<sup>-1</sup> s<sup>-1</sup>;  $\mu_e/\mu_h = 27.5$ ) as compared to the J47:ITIC blend ( $\mu_h = 1.85 \times 10^{-4}$  cm<sup>2</sup> V<sup>-1</sup> s<sup>-1</sup>;  $\mu_e/\mu_h = 2.25$ ).
- Keeping the triisopropylsilyl substituent on the DTBDT moiety copolymerized with 1,3-bis(thiophen-2-yl)-5,7-bis(2-ethylhexyl)benzo-[1,2-c:4,5-c']dithiophene-4,8-dione (BDD), Huang and collaborators obtained the PBDS-T polymer (see Figure 1, P29)). They compared it to its homologue PBDB-T with ethylhexyl branched chains (P28) [87]. UV-Vis absorption spectrometry showed that PBDS-T had a higher absorption coefficient than PBDB-T and a better crystallinity, as confirmed by low-angle X-ray diffraction. Cyclic voltammetry revealed lower HOMO and LUMO energy levels for this polymer, as suggested by density functional theory (DFT) calculations. This was attributed to  $\sigma^*(Si)-\pi^*(C)$  bond interaction leading to an effective reduction in the energy levels of the silylated polymer. Moreover, steady-state and transient photoluminescence measurements demonstrated that PBDS-T:ITIC films present an improved crystallinity relative to that of PBDB-T:ITIC. This was consistent with better photovoltaic performances for PBDS-T:ITIC that led to a PCE of 11.06% with a  $V_{OC}$  of 0.985 V, a  $J_{SC}$  of 18.68 mA cm<sup>-2</sup>, and an FF of 60% in comparison to those of PBDB-T:ITIC (PCE of 9.80% with a  $V_{OC}$  of 0.869 V, a  $J_{SC}$  of 16.58 mA cm<sup>-2</sup>, and an FF of 68%). Later on, the same authors reached higher photovoltaic performances by improving the active layer morphology through a subtle variation of the NFA structure (PCE of 12.04% with a  $V_{OC}$  of 0.88 V, a  $J_{SC}$  of 19.42 mA cm<sup>-2</sup>, and an FF of 70%) [88]. The PBDS-T polymer subsequently used in combination with BTP-eC9 as the acceptor led to solar cells with further improved PCE of 16.4% [89], here also explained by enhanced film crystallinity and nanostructured packing of PBDS-T: BTP-eC9 blends.

Polymers J71, J47, and PBDS-T all had in common that they were substituted by the same tripropylsilyl fragment.

- Another polymer containing this fragment, named as PE6 (see Figure 1, P30), with a structure close to that of J71, recently displayed a high-power conversion efficiency of 15.09% by blending with 2,2'-((2Z,2'Z)-(12,13-bis(2ethylhexyl)-3,9-diundecyl-12,13-dihydro-[1,2,5]thiadiazolo [3,4e]thieno [2,"3":4',5']thieno [2",3":4,5]pyrrolo [3,2-g]thieno [2',3':4,5]thieno [3,2-b]indole-2,1'-diyl)bis(methanylylidene))bis(5,6-difluoro-3-oxo-2,3-dihydro-1H-indene-2,1-diyldiene)dimalononitrile (Y6) as the acceptor [90]. Recently, Genene and collaborators compared the two polymers PBDTTSi-TzBI and PBDTTS-TzBI, based on DTBDT and containing alkylsilyl and alkylthio side chains, respectively, associated with an acceptor imide-fused benzotriazoles (TzBI) acceptor block, itself substituted by two invariant alkyl (ethylhexyl and octyl) chains (see Figure 1, P31, P32) [91]. Electrochemical characterization highlighted the higher propensity of the trialkylsilyl side chains to lower the HOMO level as compared to the thioalkyl ones: the HOMO/LUMO energy levels were  $-5.46/-3.33$  and  $-5.38/-3.32$  eV for PBDTTSi-TzBI and PBDTTS-TzBI, respectively. However, PBDTTS-TzBI-based devices yielded better PCE values (7.32% and 9.60%) than PBDTTSi-TzBI systems (3.98% and 6.85%), using PC71BM or ITIC as the acceptor, respectively. No particular different features were denoted by AFM or TEM examination. The best hole/electron mobilities for PBDTTS-TzBI:ITIC and PBDTTSi-TzBI:ITIC were  $9.27 \times 10^{-4}/7.32 \times 10^{-4}$  cm<sup>2</sup> V<sup>-1</sup> s<sup>-1</sup> and  $5.24 \times 10^{-4}/1.98 \times 10^{-4}$  cm<sup>2</sup> V<sup>-1</sup> s<sup>-1</sup>, respectively, showing more balanced  $\mu_h/\mu_e$  charge carrier mobilities for the alkylthio-based polymer. No specific investigations were reported on the even-odd effect of alkyl chains substituting the silicon atom on thin film structure and morphology as has been shown for alkyl-substituted small molecules [92].

### 2.5. Alkylthio Chains

- As seen just above, the introduction of a sulfur atom between the thiophene lateral moiety of the donor moiety DTBDT and an alkyl chain may have a positive effect on photovoltaic performances. This has been the subject of a specific investigation for a DTBDT-based material copolymerized with fluorinated benzothiadiazole and thiophene units (see P33–P35, Figure 1) [93]. The thiophene rings attached to the BDT core were substituted in the 4-position by a bulky *n*-decyl chain and, and in the 5-position, either by another *n*-decyl linear chain for P33, by an *n*-thiodecyl chain for P34, or by a branched 2-ethylhexyl chain for P35. The first observation was a lower solubility of P33 in 1,2-dichlorobenzene in comparison to the two other polymers. No drastic difference was observed between the optical band gaps of the three polymers (1.63 to 1.67 eV). P34 and P35 displayed similar electrochemical behaviors, but with a HOMO energy of about  $-5.7$  eV, i.e., 0.2 eV lower than that of P33, as the signature of the electronic impact of the presence of sulfur atoms. Once blended with PC<sub>71</sub>BM as the acceptor, the best performing polymer in the OPV device was P35, with a PCE of 9.0%, compared to 7.9 and 6.8% for P34 and P33, respectively, in agreement with the better balanced  $\mu_e$  and  $\mu_h$  values obtained for P35. This was explained by a difference in blend morphology revealed by AFM analysis. No phase contrast between the donor and acceptor phases was observed in P33:PC<sub>71</sub>BM films which was a sign of high miscibility of the two materials, contrarily to P34:PC<sub>71</sub>BM blend films that exhibited an average domain size of 80–90 nm of segregated phases of fullerene and polymer, responsible for charge recombination. P35:PC<sub>71</sub>BM films displayed a surface morphology compatible with an interpenetrating network well suited for generation and separation of charges, demonstrated here the advantage of using a branched chain over the thiodecyl one as the pendant thiophene substituent.
- In that spirit, Chang and collaborators proposed to test thioalkyl pendant chains for tuning the phase crystallinity of a blend and, thus, its morphology [94]. Two donor polymers were investigated, PBDB-TF used as the host polymer and PBDB-T-SF used

as the guest polymer (see **P36**, **P37**, Figure 1). Note that PBDB-TF is also known as PBDB-T-2F or more commonly as PM6, a very performant polymer that recently led to high PCE values on a large-area flexible module (up to 13.2% for 54 cm<sup>2</sup>) [95]. PBDB-TF and PBDB-T-SF presented identical backbone structures but different side chains grafted on the 5-position of the pendant thienyl rings of the DTBDT moiety, ethylhexyl for PBDB-T and thioethylhexyl for PBDB-TSF. This resulted in a difference in orientation of the side chains at the 4,8-positions of the BDT moiety that contributed to lowering the phase crystallinity of the host polymer by loading the guest polymer. Blends of polymers were associated with Y6 as the acceptor. By fine-tuning the PBDB-TF:PBDB-T-SF ratio, the authors demonstrated that it was possible to optimize the original fibrils' size, from 10–20 nm and 30–60 nm for PBDB-TF:Y6 and PBDB-T-SF:Y6 binary blends, respectively, to over 100 nm for the for PBDB-TF:PBDB-T-SF:Y6 ternary blend. This meso-scale morphology was favorable to increased and well-balanced electron and hole mobilities, leading to an improved PCE of 16.42% as compared to the PCE of 15.50% obtained for the original PBDB-TF:Y6 binary blend.

### 2.6. Influence of the Length and Linear/Branched Nature of Carbonyl Side Chain

Introducing a carbonyl function between the conjugated backbone of a polymer and an alkyl side chain is also a way to modify intermolecular interactions and thus aggregation properties of conjugated polymers [96,97]. Polymers presenting twisted conjugated skeletons, based on difluorinated DTBDT and terthiophene, have been investigated. The terthiophene unit was substituted on the 3- and 3''-positions by either an n-ethylhexyl chain (PBDT-3T), a 2-ethylhexyl ketone (PBDT-3TCO), an n-decyl ketone fragment (P3TCO-D), or a 3,7-dimethyloctyl ketone (P3TCO-DMO) as depicted in Figure 1 (**P38–P41**). Photovoltaic performances were evaluated for blends with IT-4F as the acceptor. A PBDT-3T:IT-4F-based device gave a markedly lower PCE value (1.05%) than the others (10.1 to 12.8%), that was attributed to the quality of their respective BHJ morphologies. The key parameter identified was the introduction of the function (C=O) in the structure of the polymer which led to intra/intermolecular interactions of S···O and O···H reinforcing aggregation capacity between the polymer chains and the use of an appropriate bulky chain which modulated this aggregation. Branched chains of 3,7-dimethyloctyl have been shown to be best at tuning bicontinuous phase separation and improving charge carriers' mobilities, purity, and domain size.

## 3. Small-Molecule-Based Systems

In the last decade, many efforts have been devoted to donor small molecules (DSMs) which constitute an excellent alternative to polymers from a synthetic point of view, mainly for better ease of purification and much higher batch-to-batch reproducibility, and to non-fullerene acceptors (NFAs) which allow the acquisition of a large library of acceptor materials absorbing in a wider spectral width than fullerene derivatives. It is established that the performances of OPV cells are closely linked to the conditions of preparation: active layer composition, solvent used for spin coating, thickness of BHJ, solvent annealing (SVA), etc. In order to correctly compare the systems mentioned below, we preferentially considered the cases where parent molecules were studied simultaneously and published in the same paper. When this was not the case, we compared parent molecules only if the conditions for preparing the respective OPV cells were very similar.

### 3.1. Donor Small Molecules (DSMs)

In this section, we will examine small A-D-A molecules whose structure consists in two main parts: a  $\pi$ -conjugated backbone and flexible alkyl chains. The  $\pi$ -conjugated backbone is responsible for the molecular electronic properties that determine the D or A character of the molecule to be used in the BHJ. Due to its more or less rigid character, it can also undergo  $\pi$ -stacking effects that directly influence the morphology of the active layer [98]. These molecules generally consist in a central D moiety flanked by oligothio-

phenes as the transmitter backbones, terminated by different electron-withdrawing groups. The BDT-based unit (compounds 3–10, 15–26) currently attracts particular interest as a central electron donor moiety due to its synthesis and use in OPVs in copolymers [81] and small-molecule [99] systems. A representative series of DSMs recently studied is given in Figure 3 and Table 1. Compounds 1–2 presented an in-line-type  $\pi$ -conjugated backbone, with lateral substituents of alkyl nature only, whereas compounds 26–29 had a more extended fused central fragment, the naphtho [1,2-*b*:5,6-*b'*]dithiophene (NDT), in comparison to the BDT one. The transmitter backbones consisted in a sequence of thiophene units (compounds 1–4, 9–29 and 33–35) or an alternation of thiophene and fused dithiophene or thiazolo [5,4-*d*] thiazole units (5–8 and 30–32). As terminal acceptor groups, rhodanine (1–2, 5–8, 12–35), dicyano-methylene-3-indanone (3, 4), or ester (9–11) were classically chosen: these groups are quite easily incorporated during the final step of the synthesis procedure by the Knoevenagel condensation on the terminal thiophene carbaldehyde. Processability of small molecules for OPVs is a limiting factor because they often present a great tendency to crystallize. To circumvent this drawback, the common way is to introduce alkyl-based side chains onto their  $\pi$ -conjugated backbone. As will be presented later on, the nature (linear or branched) and position of the alkyl chains, (i) in the central, (ii) lateral, and/or (iii) terminal position of the molecular structure may have a great impact on the morphology of the resulting BHJs and, thus, on their photovoltaic performances.

The acceptor organic semiconductors evoked in this part and absent from Figure 2 are represented in Figure 4.

### 3.1.1. Alkyl Chains in the Central Position of the Molecule

- Introduction of central alkyl chains along the conjugated backbone of DSMs may help in reducing strong aggregation and optimizing morphology. Duan and collaborators recently examined the effect of substituting the rigid indaceno [1,2-*b*:5,6-*b'*]dithiophene (IDT) central core by isomeric branched or linear chains in DSMs with conjugate backbones consisted in fluorinated/octylated terthienyl fragments and end-capped by 3-ethylrodanine (see Figure 3, molecules 1–2) [100]. The nature of the alkyl chain, either 2-ethylhexyl branched (molecule 1 named as I4FR-EH) or *n*-octyl linear (molecule 2 named as I4FR-O), did not influence the electronic parameters (HOMO/LUMO levels) evaluated by UV-Vis spectroscopy and electrochemistry. Interestingly, the photovoltaic parameters revealed a PCE twice as high for the DSM with the central branched chains as for that with linear chains (see entries 1–2 in Table 1). This was explained by morphology (studied by TEM) and charge-transport (measured by SCLC mobility) characterizations that revealed a fine donor-acceptor mixture for I4FR-EH:PC<sub>71</sub>BM blends as compared to the presence of diffused I4FR-O clusters across the I4FR-O:PC<sub>71</sub>BM thin film and better balanced electron ( $1.48 \times 10^{-4}$  vs.  $1.59 \times 10^{-4} \text{ cm}^2 \text{ V}^{-1} \text{ s}^{-1}$ ) and hole ( $1.23 \times 10^{-4}$  vs.  $1.13 \times 10^{-4} \text{ cm}^2 \text{ V}^{-1} \text{ s}^{-1}$ ) mobilities for I4FR-EH:PC<sub>71</sub>BM and I4FR-O:PC<sub>71</sub>BM, respectively.

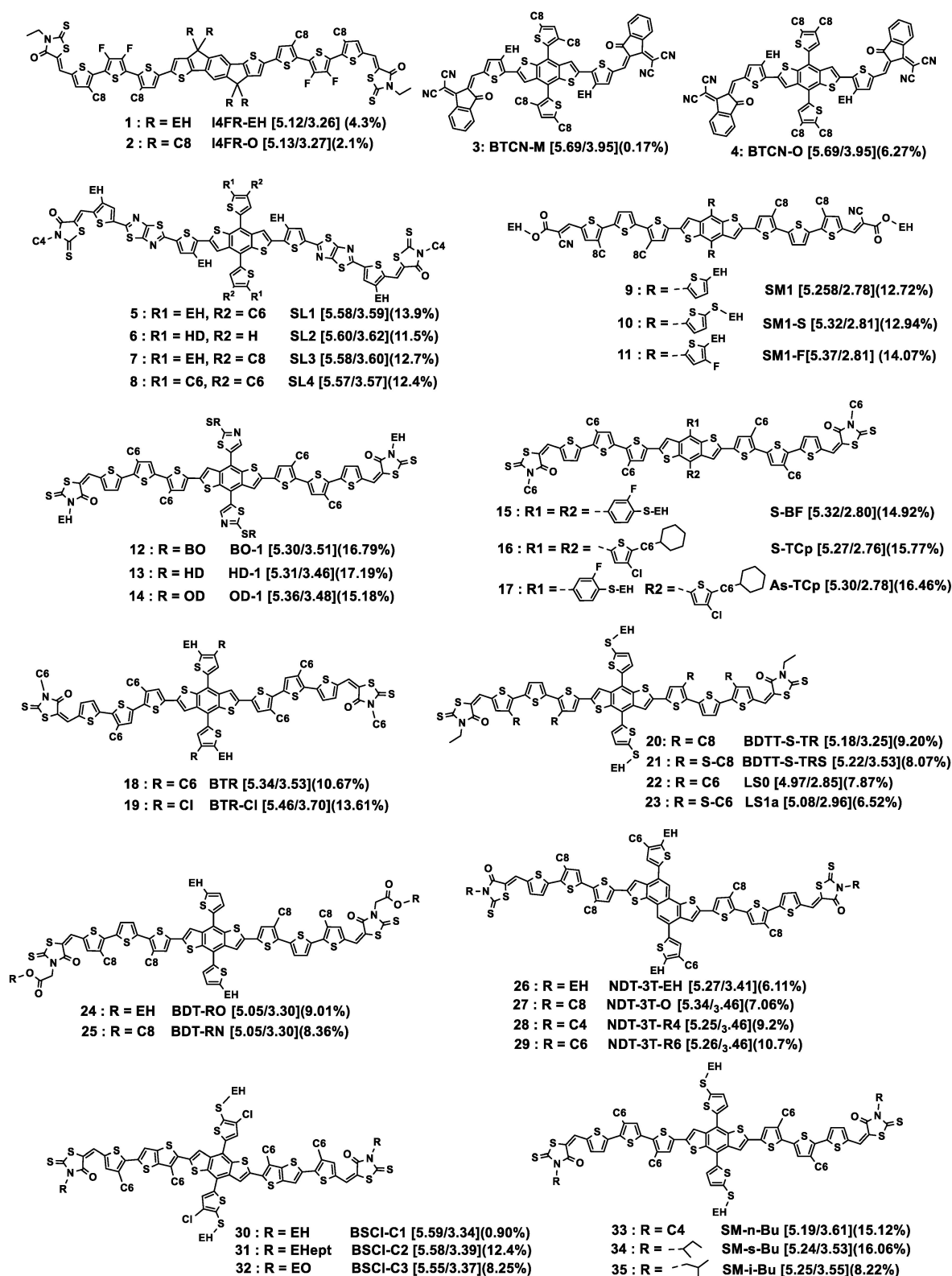


**Figure 3.** Chemical structures of donor small molecules discussed in this section. HOMO/LUMO energy levels (eV) are given in square brackets. The best PCE value obtained for each compound is indicated in parentheses. For full OPV parameters, see Table 1. EH: 2-ethylhexyl; EHept: 3-ethylheptyl; EO: 4-ethyloctyl; HD: 2-hexyldecyl; BO: 2-butylloctyl; OD: 2-octyldodecanyl. Cx: *n*-alkyl linear chain with x methylene units.

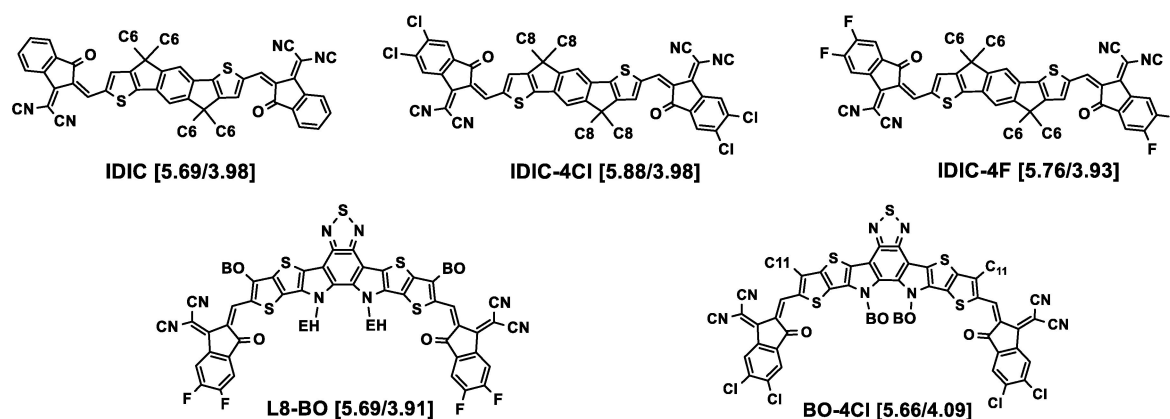


**Figure 4.** Chemical structures of acceptor molecules cited in this section and absent from Figure 2. HOMO/LUMO energy levels (eV) are given in square brackets. BO = 2-butyloctyl.

- Recently, Liu and collaborators have investigated the effect of the position of central alkyl chains grafted on the pendant thiophene of the DTBDT unit on the performance of small molecules [101]. They chose a compact molecular structure, consisting of a central DTBDT core surrounded on each side by a thiophene ring and end-capped by 2-(3-oxo-2,3-dihydro-1H-inden-1-ylidene) malononitrile (DCI) units. The difference between the two synthesized molecules was the position of two *n*-octyl chains introduced onto the thiophene ring, in the 4- and 5-position (“ortho” substitution) in the case of BTCN-O and in the 3- and 5-position (“meta” substitution) for BTCN-M (see Figure 3, molecules 3–4). This subtle adjustment resulted in different HOMO energy levels of  $-5.59$  and  $-5.69$  eV for BTCN-O and BTCN-M, respectively, with their LUMO energy levels unchanged ( $-3.95$  eV). This was related to a torsion effect on the pendant thiophene units from the DTBDT core, as anticipated by theoretical calculations and confirmed by GIWAXS measurement. Consequently, BTCN-O underwent compact and strong intermolecular  $\pi$ – $\pi$  stacking with highly ordered lamellar packing while BTCN-M exhibited weak intermolecular  $\pi$ – $\pi$  interaction and no ordered lamellar packing. This strongly impacted the photovoltaic performance since BTCN-O acted as an electron donor (see Table 1, entries 3, 3 bis) while BTCN-M behaved more as an electron acceptor (see Table 1, entries 4, 4 bis). Photophysical characterizations were later performed on BHJs in which both BTCN-O and BTCN-M were associated with PC<sub>71</sub>BM as the acceptor then with PBDB-T as the donor [102]. These investigations highlighted the crucial role of the more or less twisted molecular conformation of BTCN-O and BTCN-M in the morphology of the blends, which was strongly dependent on the  $\pi$ – $\pi$  stacking capacity of each molecule, thus explaining the dramatic discrepancy in device performance.
- Using a less compact  $\pi$ -conjugated backbone, Wang and collaborators obtained different effects when varying the length and nature of the central alkyl chains [103]. The molecules under study had a central DTBDT donor moiety, surrounded by TTz and thiophene units and end-capped by a butyl substituted rhodanine acceptor group. Branched and linear alkyl chains of varying lengths were introduced onto the 4- and 5-positions of the pendant thiophene rings of the DTBDT moiety (see Figure 3, molecules 5–8). As a consequence, they presented close HOMO/LUMO levels and similar UV–visible features in thin films. Interestingly, using Y6 as the acceptor, the best mobility values were obtained for the blend film based on SL1 with *n*-hexyl and ethylhexyl chains, with well-balanced hole and electron mobilities ( $\mu_h = 3.82 \times 10^{-4} \text{ cm}^2 \text{ V}^{-1} \text{ s}^{-1}$  and  $\mu_e = 3.74 \times 10^{-4} \text{ cm}^2 \text{ V}^{-1} \text{ s}^{-1}$ ), while the worst results were obtained for the blend based on the SL2 molecule bearing only one hexyldecyl chain ( $\mu_h = 1.96 \times 10^{-4} \text{ cm}^2 \text{ V}^{-1} \text{ s}^{-1}$  and  $\mu_e = 1.72 \times 10^{-4} \text{ cm}^2 \text{ V}^{-1} \text{ s}^{-1}$ ). The blends based on the two other molecules, SL3 and SL4 with ethylhexyl/*n*-octyl

and two n-hexyl chains, respectively, presented intermediate results. Photovoltaic parameters revealed very similar  $V_{OC}$  values (near to 0.88 eV) whereas the device based on SL1 exhibited the best maximum values of  $J_{SC}$  ( $22.6 \text{ mA cm}^{-2}$ ), FF (68%), and PCE (13.9%). The SL2 molecule led to the lowest values of  $J_{SC}$  ( $21.5 \text{ mA cm}^{-2}$ ), FF (60%), and PCE (11.15%). The devices based on SL3 and SL4 offered intermediate parameters (see Table 1, entries 5–8). Morphology characterization by AFM, TEM, and GIWAXS examination showed that mixing branched and linear chains (SL1 and SL3) improved the crystallinity of the blend. SL2 with only one chain per thiophene ring presented higher phase separation with the Y6 acceptor. For the other di-alkylated molecules, the longer the alkyl chain, the better the compatibility with Y6.

- As already demonstrated for donor polymers, the use of alkylthio side chains, especially when introduced onto the pendant thiophene of the central donor moiety, may contribute to tuning the HOMO energy level of the  $\pi$ -conjugated material in such a way that improved photovoltaic parameters can be obtained. This was also demonstrated by Qiu and collaborators for DSMs with molecules **9** (named as SM1) and **10** (named as SM1-S) depicted in Figure 3 [104]. The SM1-S molecule with a central ethylhexylthio substituent exhibited lower HOMO/LUMO levels of  $-5.32$  and  $-2.81$  eV, respectively, than the SM1 molecule with a central ethylhexyl substituent ( $-5.25$  and  $-2.78$  eV, respectively), better balanced  $\mu_e$  and  $\mu_h$  values when blended with Y6 as the acceptor, and better photovoltaic performance than SM1 (12.94% and 12.72%, respectively). The molecular structure was further improved by the introduction of a fluorine atom onto the thiophene ring, and the resulting device based on the SM1-F:Y6 blend exhibited a higher PCE of 14.07% (see Table 1, entries 9–11).
- Alkylthio side chains have been also introduced onto pendant thiazole units, used in place of the thiophene (see Figure 3, molecules **12–14**) [105]. In this case, the authors have tested the length of branched alkyl chains, from the 2-butyloctyl to 2-hexyldecyl and 2-octyldecyl introduced in the central part of molecules BO-1, HD-1, and OD-1, respectively. Whereas only slight differences were obtained between their UV-Vis spectra in solution or as thin films and their HOMO/LUMO levels, GIWAXS measurements revealed a greater content of face-on orientation with the elongation of the alkyl chain, attested by an increase in their coherence length of  $\pi$ - $\pi$  stacking in the out-of-plane direction from 46.19 Å to 48.18 Å to 50.81 Å for BO-1, HD-1, and OD-1, respectively. After blending with the non-fullerene acceptor BTP-eC9, it appeared that all blend films showed a preferred face-on orientation, with the largest coherence length of  $\pi$ - $\pi$  stacking in the out-of-plane direction for HD-1-based film (49.46 Å). The hole/electron mobilities of the blends were  $1.03 \times 10^{-3}/1.23 \times 10^{-3} \text{ cm}^2 \text{ V}^{-1} \text{ s}^{-1}$ ,  $1.14 \times 10^{-3}/1.32 \times 10^{-3} \text{ cm}^2 \text{ V}^{-1} \text{ s}^{-1}$ , and  $0.99 \times 10^{-3}/1.18 \times 10^{-3} \text{ cm}^2 \text{ V}^{-1} \text{ s}^{-1}$  for BO-1:BTP-eC9, HD-1:BTP-eC9, and OD-1:BTP-eC9, respectively. As a result, the HD-1-based device yielded the best PCE value of 17.19% with a  $V_{OC}$  of 0.842 V, a  $J_{SC}$  of  $26.04 \text{ mA cm}^{-2}$ , and an FF of 78.46% (see Table 1, entries 12–14).
- A strategy for improving the crystallinity of active layers is to introduce asymmetry in the active molecules. Towards that aim, small molecules with symmetric/asymmetric cyclopentyl-hexyl side chains were recently designed and compared with their analogue S-BF-containing symmetric phenyl thioalkyl side chains (see Figure 3, molecules **15–17**) [106]. Estimation of the Flory–Huggins interaction parameter via contact angle measurement suggested that miscibility with the chosen acceptor, L8-BO, can be elevated by use of the cyclopentyl-hexyl chain, as anticipated by use of computational simulation at the B3LYPD3/Def2-SVP level of theory that suggested stronger intermolecular interactions for the As-TCp:L8-BO and S-TCp:L8-BO mixtures. GIWAXS analyses of the three blends revealed textures comprising primarily face-on and some edge-on crystallites, favorable to 3D charge pathways. The calculated crystal coherence lengths of the blends in the out-of-plane direction were 136.2 Å, 88.5 Å, and 72.8 Å for S-BF:L8-Bo, AsTCp:L8-Bo, and S-TCp:L8-Bo, respectively. The best photovoltaic parameters were obtained, however, for AsTCp:L8-Bo (see Table 1, entries



15–17) which was explained by a favorable balance between aggregation behavior and balanced A/D miscibility.

- Besides this work on alkyl chains, it is worth noting that, in their quest for controlling phase separation in blend films through liquid crystalline molecular structure design, Chen and collaborators found out that replacing an *n*-hexyl chain of the DTBDT core of a nematic liquid crystalline molecule (Figure 3, molecule 18) by a chlorine atom not only contributed to lowering the energy levels, making them more compatible with those of Y6, but also to modifying in a favorable way the liquid crystalline pattern [107]. The obtained molecule, named as BTR-Cl (see Figure 3, molecule 19), not only led to the formation of mixed edge-on and face-on  $\pi$ - $\pi$  arrangements in BTR-Cl:Y6-blended films as well as its parent, the BTR molecule, but also underwent optimal phase separation and film morphology, contributing to boosting each photovoltaic parameter (see Table 1, entries 18–19). Later on, this was improved by active layer optimization through fine variation of the concentration of the casted solution (PCE increased to 14.7%) or adding 5% PC<sub>71</sub>BM in the BTR-Cl:Y6 blend (record PCE of 15.34%) [108,109].

### 3.1.2. Alkyl Chains in the Lateral Position of the Molecule

- The effect of substituting thiophene rings belonging to the transmitter backbone by thioalkyl chains instead of *n*-alkyl chains has been investigated in the following example involving molecules 20–23 (see Figure 3), the pendant thiophene of DTBDT being invariantly substituted by a thioethylhexyl branched chain [110–112]. After blending each DSM with PC<sub>71</sub>BM with the same ratio (1:0.8), it was observed that introducing an S atom between the alkyl chain and the transmitter backbone resulted in a slight effect on the HOMO energy level and in an undesirable effect on the photovoltaic performances: for *n*-octyl chains, the presence of the S atom contributed to lowering the PCE value from 9.20% (molecule 23: BDTT-S-TR) to 8.07% (molecule 21: BDTT-S-TRS). The same tendency was observed for the *n*-hexyl chain (PCE diminished from 7.87% for molecule 22 (named as LS0) to 6.52% for molecule 23 (named as LS1a)). It is also noteworthy that in this case, with or without an intermediate S atom, the longer the linear chain, the better the photovoltaic parameters (see Table 1, entries 20 and 22 vs. entries 21 and 23, respectively).

### 3.1.3. Alkyl Chains in the Terminal Position of the Molecule

- Introducing alkyl chains at the extremities of DSMs for improving solubility also modified molecular packing and photovoltaic performances. The so-called DR3 molecule (first known as DR3TBDTT), thoroughly investigated since its first description [99], has inspired the synthesis of molecules 24 and 25, named as BDT-RO and BDT-RN, respectively (see Figure 3) [113]. Their structures were very similar to that of DR3, with a DTBDT core as the central D unit and terthiophene partially substituted by *n*-octyl chains as the  $\pi$ -conjugated transmitter unit, but the two rhodanine end moieties have been esterified by using either the ethylhexyl branched chain for BDT-RO or the *n*-octyl linear alkyl chain for BDT-RN. They presented HOMO/LUMO energy levels (5.05 and 3.30 eV, respectively) insensitive to the branched or linear nature of the terminal alkyl chains and very close to those of DR3. It was concluded that replacing alkylated with esterified rhodanine introduces only marginal changes in the energetics of the DSMs. BDT-RO active layers displayed more separated D-A networks and better hole and electron mobilities ( $3.24 \times 10^{-4}$  and  $6.45 \times 10^{-4}$  cm<sup>2</sup> V<sup>-1</sup> s<sup>-1</sup>, respectively) than BDT-RN BHJs ( $1.87 \times 10^{-4}$  and  $5.44 \times 10^{-4}$  cm<sup>2</sup> V<sup>-1</sup> s<sup>-1</sup>, respectively). Consequently, photovoltaic parameters were better for BDT-RO-based solar cells than for BDT-RN (see Table 1, entries 24, 25).
- Another comparative study has been conducted on molecules containing the more rigid conjugated naphtho [1,2-*b*:5,6-*b'*]dithiophene (NDT) central core instead of the BTD one and with alkylated rhodanine as terminal fragments (see Figure 3, molecules 26–29) [114]. In that case, using end-branched alkyl chains (molecule 26: NDT-3TEH)

resulted in higher HOMO energy levels for NDT-3TEH than for NDT-3T-O (molecule 27), of  $-5.27$  eV vs.  $-5.34$  eV, and higher LUMO energy levels, of  $-3.41$  eV vs.  $-3.46$  eV. This slight offset was attributed to the reduced molecular aggregation state in the case of the use of terminal branched alkyl chains instead of linear chains. NDT-3T-EH:IDIC-4F blend films exhibited non-uniform domain sizes, whereas NDT-3T-O:IDIC-4F blend films presented a bicontinuous and regular interpenetrating network and a preferred edge-on orientation stacking, as characterized by AFM and GIWAXS analyses. These results were in accordance with lower hole and electron mobilities for NDT-3T-EH active layers ( $5.60 \times 10^{-4}$  and  $1.69 \times 10^{-4}$   $\text{cm}^2 \text{V}^{-1} \text{s}^{-1}$ , respectively) than for NDT-3T-O ( $1.69 \times 10^{-4}$  and  $1.21 \times 10^{-3}$   $\text{cm}^2 \text{V}^{-1} \text{s}^{-1}$ , respectively). In that case, the molecule with end linear alkyl chains led to the best photovoltaic figures (see Table 1, entries 26–29).

- Further investigations on the length of terminal alkyl chains led to the obtention of liquid crystalline phases by using *n*-butyl and *n*-hexyl linear terminal chains (see Figure 3, molecules 28,29) [115]. The resulting molecules named as NDT-3T-R4 and NDT-3T-R6, respectively, adopted not only the edge-on orientation like their NDT-3TEH and NDT-3T-O counterparts but also face-on orientation. After blending with IDIC-4F as the acceptor, the liquid crystalline characters of the molecules helped in efficient phase separation in the active layer, with only face-on orientation in the two blends. Interestingly, improved photovoltaic parameters were obtained (see Table 1, entries 13–14).
- Tuning the branching point in terminal alkyl chains is also an option for branched chain investigation. Wu and collaborators synthesized SDMs with a chlorinated BDT core surrounded by thiophene-based transmitters and end-capped with alkylated rhodanine terminal acceptor groups [116]. The final alkyl chains were of a branched nature, with an ethyl fragment grafted on the 2nd, 3rd, and 4th position of hexyl (BSCI-C1), heptyl (BSCI-C2), or octyl (BSCI-C3) main chains, respectively (see Figure 3, molecules 30 to 32). UV–visible spectra of thin films of these molecules suggested improved molecular interactions and stronger molecular  $\pi$ – $\pi$  stacking for the C2-derivative, whereas the bandgap had a tendency to slightly narrow from BSCI-C1 to BSCI-C3. The best hole and electron mobilities of active layers were measured for BSCI-C2 ( $3.83 \times 10^{-4}$  and  $1.37 \times 10^{-4}$   $\text{cm}^2 \text{V}^{-1} \text{s}^{-1}$ , respectively) which also afforded the best photovoltaic parameters as can be seen in Table 1, entries 30–32. GIWAXS characterization of pure films suggested that outward shifting branching points resulted in an increasing crystallinity and order range. After blending with IDIC-4Cl as the acceptor, BSCI-C2 formed the strongest intermolecular D–A interaction. As a result, the BSCI-C2:IDIC-4Cl blend afforded the best photovoltaic parameters as presented in Table 1, entries 30–32.
- Drastic improvement in this field has been recently reached with the synthesis and study of a series of isomeric SMDs based on the benzodithiophene-terthiophene core with linear, 1st carbon, and 2nd carbon position branched butyl-based rhodanine, respectively (see Figure 3, molecules 33–35) [117]. The isomeric terminal alkyl chain proved to have clear influence on blend film morphology, using BO-4Cl as the acceptor. SM-s-Bu:BO-4Cl blend films exhibited the more favorable blend morphology with nanofiber-based phase separation containing BO-4Cl microcrystals. Higher and more balanced charge mobilities were found for the SM-s-Bu:BO-4Cl blend ( $\mu_e/\mu_h = 6.50 \times 10^{-4}/7.26 \times 10^{-4}$   $\text{cm}^2 \text{V}^{-1} \text{s}^{-1}$  vs.  $4.91 \times 10^{-4}/6.00 \times 10^{-4}$   $\text{cm}^2 \text{V}^{-1} \text{s}^{-1}$  and  $3.13 \times 10^{-4}/4.63 \times 10^{-4}$   $\text{cm}^2 \text{V}^{-1} \text{s}^{-1}$  for SM-n-Bu:BO-4Cl and SM-i-Bu:BO-4Cl, respectively). Consistently, this blend led to the best photovoltaic parameters with a PCE up to 16.06% (see Table 1, entries 33–35). This example highlights once again the high sensitivity of morphology and photovoltaic parameters to the isomer form of the final alkyl chains.

**Table 1.** Photovoltaic performances of donor small molecules <sup>a</sup>.

Entry	Active Layer	Solvent	Additional Conditions	$\mu\text{h}/\mu\text{e}^{\text{b}}$ $10^{-4} \text{ cm}^2$ $\text{V}^{-1} \text{ s}^{-1}$	$V_{\text{OC}}^{\text{c}}$ (V)	$J_{\text{SC}}^{\text{c}}$ (mA $\text{cm}^{-2}$ )	FF <sup>c</sup> (%)	PCE <sup>c</sup> (%)	Ref.
1	I4FR-EH:PC <sub>71</sub> BM	CF	SVA <sup>e</sup> : DCM 20 s	1.23/1.48	0.9	8.8	48	4.3	[100]
2	I4FR-O:PC <sub>71</sub> BM	CF	SVA: DCM 20 s	1.13/1.59	0.85	6.1	32	2.1	[100]
3	BTCN-M:PBDB-T	CF	-	~0.10/~0.002	0.98	12.03	50	5.89	[101]
3 bis	BTCN-M:PC <sub>71</sub> BM	CF	-	0.13/0.19	1.10	0.62	43	0.29	[101]
4	BTCN-O:PBDB-T	CF	-	~0.10/~0.002	0.95	5.04	34	1.62	[101]
4 bis	BTCN-O:PC <sub>71</sub> BM	CF	-	0.80/0.26	0.97	11.68	59	6.68	[101]
5	SL1:Y6	CF	SVA: CS <sub>2</sub> 90 s	3.82/3.74	0.88	22.6	68	13.9	[103]
6	SL2:Y6	CF	SVA: CS <sub>2</sub> 90 s	1.96/1.72	0.89	21.5	60	11.15	[103]
7	SL3:Y6	CF	SVA: CS <sub>2</sub> 90 s	2.78/2.58	0.88	21.6	67	12.7	[103]
8	SL4:Y6	CF	SVA: CS <sub>2</sub> 90 s	2.41/2.19	0.87	23.0	62	12.4	[103]
9	SM1:Y6	CF	TA <sup>f</sup> 120 °C 10 min	1.78/4.12	0.805	23.59	67.0	12.72	[104]
10	SM1-S:Y6	CF	TA 120 °C 10 min	1.87/3.67	0.825	23.23	67.7	12.94	[104]
11	SM1-F:Y6	CF	TA 120 °C 10 min	3.69/3.87	0.866	23.25	69.7	14.07	[104]
12	BO-1:BTP-eC9	CF	n a	10.3/12.3	0.845	25.56	77.74	16.79	[105]
13	HD-1:BTP-eC9	CF	n a	11.4/13.2	0.842	26.04	78.46	17.19	[105]
14	OD-1:BTP-eC9	CF	n a	9.9/11.8	0.828	25.49	71.89	15.18	[105]
15	S-BF:L8-Bo	CF	SVA: CF 30 s	4.25/2.67	0.868	22.91	69.39	14.92	[106]
16	S-TCp:L8-Bo	CF	SVA: CF 30 s	3.40/2.91	0.870	23.88	73.83	15.77	[106]
17	AS-TCp:L8-Bo	CF	SVA: CF 30 s	4.55/4.25	0.873	24.45	74.90	16.46	[106]
18	BTR:Y6	CM	TA 100 °C 10 min	3.01/2.10	0.85	15.37	66.56	10.67	[107]
19	BTR-Cl:Y6	CM	TA 100 °C 10 min	2.72/2.55	0.86	22.25	56.4	13.61	[107]
20	BDTT-S-TR:PC <sub>71</sub> BM	CF	SVA: DCM 15 s	6.57/7.63	0.97	13.45	70.5	9.20	[110]
21	BDTT-S-TRS:PC <sub>71</sub> BM	CF	SVA: CF 15 s	1.91/3.51	0.87	13.14	70.5	8.07	[111]
22	LS0:PC <sub>71</sub> BM	n a <sup>d</sup>	SVA: CF 30 s	2.50/1.06	0.909	13.83	62.64	7.87	[112]
23	LS1a:PC <sub>71</sub> BM	n a	SVA: SVA:	3.15/2.37	0.851	13.15	58.27	6.52	[112]
24	BDT-RO:IDIC	CF	SVA: CS <sub>2</sub> 20 s	3.24/6.45	0.88	24.17	65.5	9.01	[113]
25	BDT-RN:IDIC	CF	SVA: CS <sub>2</sub> 20 s	1.87/5.44	0.87	14.85	64.88	8.36	[113]
26	NDT-3T-EH:IDIC-4F	CF	TA 100 °C 10 min	5.60/1.69	0.77	14.28	54.41	6.11	[114]
27	NDT-3T-O:IDIC-4F	CF	TA 100 °C 10 min	1.69/12.1	0.79	15.02	59.58	7.06	[114]
28	NDT-3T-R4:IDIC-4F	CF	TA 100 °C 10 min	3.01/2.42	0.76	17.02	71.4	9.1	[115]
29	NDT-3T-R6:IDIC-4F	CF	TA 100 °C 10 min	3.69/3.12	0.78	18.89	72.8	10.4	[115]
30	BSCI-C1:IDIC-4Cl	CF	SVA: THF 40 s	4.17/1.02	0.56	4.90	33.9	0.90	[116]
31	BSCI-C2:IDIC-4Cl	CF	SVA: THF 40 s	3.83/1.37	0.86	20.1	71.3	12.4	[116]
32	BSCI-C3:IDIC-4Cl	CF	SVA: THF 40 s	1.58/3.89	0.87	14.2	67.0	8.25	[116]
33	SM-n-Bu:BO-4Cl	CF	SVA: CB 80 s	6.00/4.91	0.830	25.26	72.12	15.12	[117]
34	SM-s-Bu:BO-4Cl	CF	SVA: CB 80 s	7.26/6.50	0.841	25.69	74.34	16.06	[117]
35	SM-i-Bu:BO-4Cl	CF	SVA: CB 80 s	4.63/3.13	0.814	18.26	55.31	8.22	[117]

<sup>a</sup> Structures of DSMs are provided in Figure 3. <sup>b</sup> Blend charge mobilities. <sup>c</sup> Data of the best performances when reported; otherwise, average values. <sup>d</sup> Not afforded. <sup>e</sup> SVA: solvent annealing. <sup>f</sup> TA: thermal annealing. DCM: dichloromethane, CF: chloroform, THF: tetrahydrofuran, CM: chloromethane, CS<sub>2</sub>: carbon disulfide, CB: chlorobenzene.

### 3.2. Non-Fullerene Acceptors (NFAs)

Despite intensive works on the well-known P3HT:PCBM system in the last two decades, the resulting devices exhibit limited average PCE values of 4–5% [118], without exceeding 7% [119,120], due to modest short-circuit current densities ( $J_{\text{SC}}$ ) and open-circuit voltages ( $V_{\text{OC}}$ ), peaking at values of 12 mAcm<sup>-1</sup> and 0.66 V, respectively [119]. To overcome these limitations, research has been oriented towards finding NFAs to be associated with P3HT and presenting strong and broad absorption from visible to near-infrared regions as well as appropriate energy levels. For systems based on P3HT, this resulted in boosted values of  $J_{\text{SC}}$  and  $V_{\text{OC}}$  leading to improved PCE values [121] up to a recent record of 10.24% [122]. Besides photophysical and electronic property studies on NFAs, solubility issues and morphology control have been addressed through side chain engineering. Very quickly, new efficient NFAs have been associated with a myriad of polymers, resulting in difficult direct comparison between NFAs due to the variety of donor polymers used. In the following, we will endeavor to compare the performance of various NFAs when used in similar conditions. There are several families of NFAs, based

on two-dimensionally  $\pi$ -conjugated core units, like phthalocyanines, subphthalocyanines, porphyrins, perylene and naphthalene diimides diketopyrrolopyroles, and more recently rigid fused-ring  $\pi$ -systems. They have inspired hundreds of papers and have been reviewed almost exhaustively until very recently [7,30,123–132]. The impressive number of review articles listed recently testifies to the enthusiasm aroused by these molecules. In this section, we will discuss very recent and non-reviewed, as far as we know, works on the last class of NFAs. As for donor polymers and small molecules, the molecular structure of NFAs, generally based on D-A alternation, is of great importance for tuning electronic parameters; the substituent engineering is also crucial for tuning the morphology of BHJ layers. Rigid fused-ring  $\pi$ -systems are frequently based on indacenodithiophene building blocks, consisting in seven-ring-fused dihydrodithieno [2,3*d*:2',3'-*d'*]-*s*-indaceno [1,2-*b*:5,6-*b'*]dithiophene (IT) or in five-ring-fused dihydro-*s*-indaceno [1,2-*b*:5,6-*b'*]dithiophene (ID) and a dithienothiophen [3,2-*b*]-pyrrolobenzothiadiazole (TPBT) central core. They gave rise to three iconic molecules in the OPV field, namely ITIC [133], IDIC [134], and Y6 [69], whose structures are given in Figure 5.

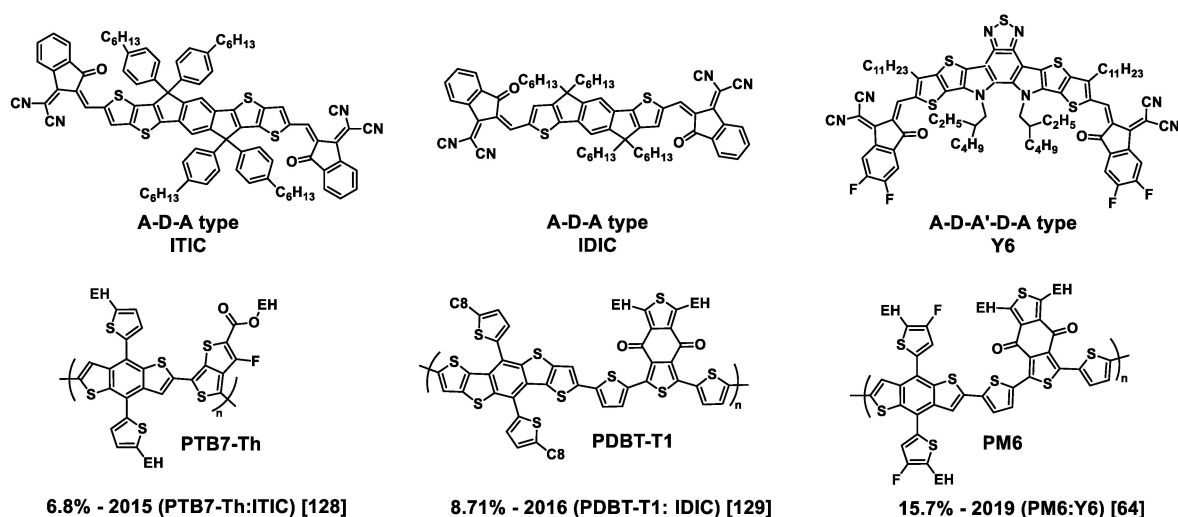


**Figure 5.** Molecular structures of ITIC, IDIC, and Y6 (top) and their first associated donor polymers (bottom). The original PCEs obtained with each compound and the years of their first description are indicated according to the corresponding references.

In 2015, Y. Lin et al. opened the way to these innovative and efficient NFAs with the first publication of the low-bandgap ITIC molecule which displayed a PCE of 6.80% by blending with the PTB7-Th donor polymer [133]. Since this first result, by changing the donor polymer and introducing electron-withdrawing halogen atoms on the end-cap groups of the ITIC molecule, together with side chain engineering, improved performances were obtained, i.e., PCEs up to 15.1% and 13.76% for an IT-4F- and an IT-4Cl-based solar cell, respectively, in 2019, and up to 15.57% for an IMC6-4F-based solar cell in 2020 (Figure 6) [135–140].

One year after the synthesis of ITIC, the same authors obtained a smaller planar fused-ring NFA, named at that time as IC-C6IDT-IC, and later on as IDIC [134]. Whereas its central core is less extended than that of ITIC, IDIC exhibited in dichloromethane strong absorption in the 500–800 nm region with a higher maximum extinction coefficient of  $2.4 \times 10^5 \text{ M}^{-1} \text{ cm}^{-1}$  (in comparison to  $1.3 \times 10^5 \text{ M}^{-1} \text{ cm}^{-1}$  for ITIC) at 664 nm. On the other hand, it afforded higher electron mobilities, measured using the SCLC method, of up to  $1.1 \times 10^{-3} \text{ cm}^2 \text{ V}^{-1} \text{ s}^{-1}$ , as compared to  $3.0 \times 10^{-4} \text{ cm}^2 \text{ V}^{-1} \text{ s}^{-1}$  for ITIC. This molecule, associated with the BDBT-T1 donor polymer, led to an improved PCE of 8.71% [134].

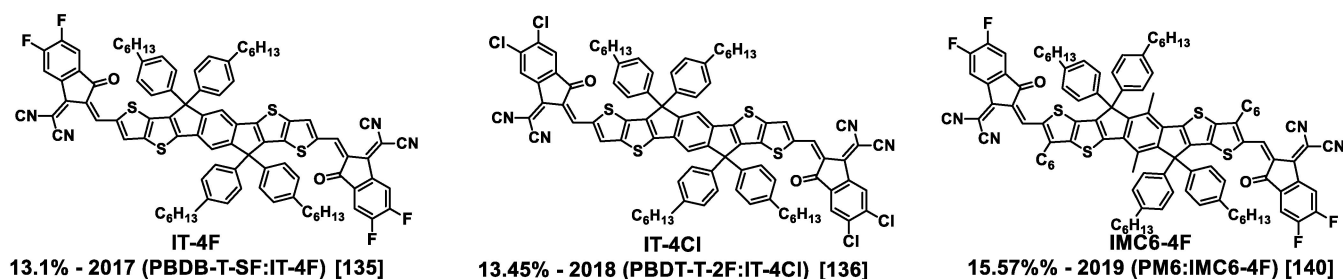


**Figure 6.** Structure of halogenated ITIC derivatives IT-4Cl, IT-4F, and IMC6-4F; their first reported record PCE and the years of their first description are indicated according to the corresponding references. The composition of the corresponding blends is given in parentheses.

Another breakthrough in NFA engineering was achieved in 2019 by Yuan and collaborators [69,141] who synthesized two new molecules, Y5 and Y6, based on a central benzothiadiazole large and planar fused ring, with an enhanced delocalization of  $\pi$ -electrons through their A-D-A'-D-A structure. The difference between them was that Y5 was substituted by four ethylhexyl chains on its central core, whereas Y6 had two ethylhexyl side chains on the pyrrole sub-units and two *n*-undecyl linear chains on the thiophene one and was substituted by two fluorine atoms on each terminal phenyl ring of the molecule. The absorption onset of the Y5 film was located at 900 nm ( $E_g = 1.38$  eV), whereas that of Y6 was located at 931 nm ( $E_g = 1.33$  eV). Optimized PBDB-T:Y5 and PM6:Y6 blend films showed a preferred face-on orientation with  $\pi$ - $\pi$  stacking in the out-of-plane direction, and, interestingly, Y6 also exhibited a remaining backbone ordering in the in-plane direction in the blend, which was not reported for Y5. It resulted in an improvement in the photovoltaic parameters obtained with the Y6-based devices in comparison to Y5 (see Table 2, entries 7, 8). Consecutively to this work, Li and collaborators tried to improve the OPV parameters by modifying Y5 and Y6 structures through adding supplementary fused phenyl rings at the two extremities of the molecules. Better PCE values were obtained with the so-called BT-BO-L4F molecule after supplementary modification consisting in replacing the central 2-ethylhexyl chains of Y6 by 2-butyloctyl chains (see Table 2, entry 9) [142]. In recent years, NFAs have inspired hundreds of papers and have been reviewed almost exhaustively until very recently [7,30,123–132]. The impressive number of review articles listed recently testifies to the enthusiasm aroused by these molecules. In the following, we will discuss very recent results about alkyl chain engineering on NFAs, the corresponding molecules are presented in Figure 7. The donor polymers mentioned in this part and absent from figures above are represented in Figure 8.

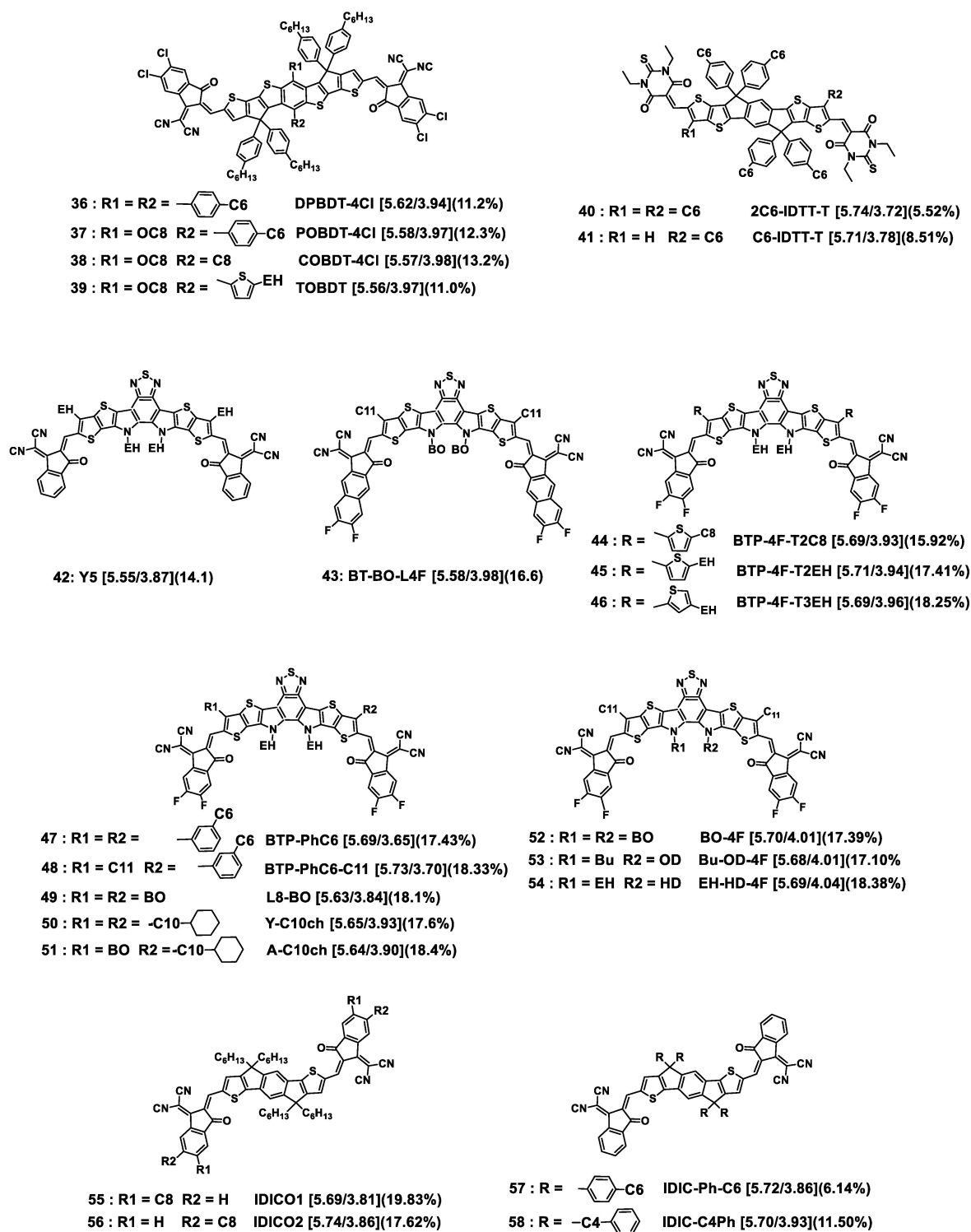


**Figure 7.** Chemical structures of non-fullerene acceptors discussed in this section. HOMO/LUMO energy levels are given in square brackets. The best PCE value obtained for each compound is indicated in parentheses. For full OPV parameters, see Table 2. EH = 2-ethylhexyl; BO = 2-butyloctyl; OD = 2-octyldodecyl; Bu = 2-butyl; HD = hexyldecyl. Cx = *n*-alkyl linear chain with *x* methylene units.

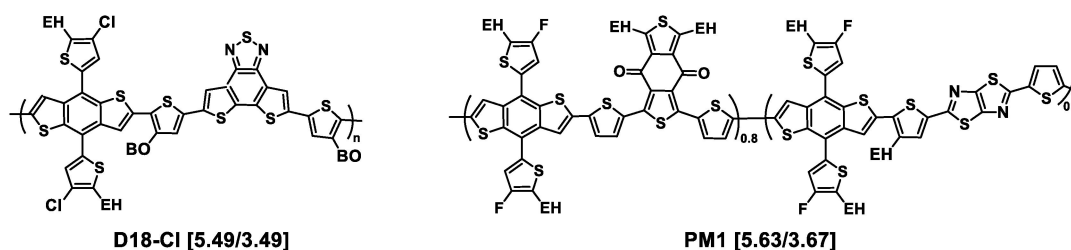


**Figure 8.** Chemical structures of donor polymers cited in this section and absent from figures above. HOMO/LUMO energy levels are given in square brackets.

### 3.2.1. Introducing Asymmetry via Central Side Chains

- Exploring the asymmetric side chain strategy [143], the teams of X. Peng and A.K.-Y. Jen investigated IT-4Cl-like compounds with a central BDT unit instead of indacene (see Figure 7, molecules 36–39) and different substituents on the central phenyl ring [144,145]. Whereas DPBDT-4Cl was substituted by two phenylhexyl side chains, POBDT-4Cl, COBDT-4Cl, and TOBDT exhibited asymmetric structures with (octyloxy; phenylhexyl), (octyloxy; *n*-octyl), and (octyloxy; ethylhexylthiophenyl) substituents, respectively. Thin films of the asymmetric compounds exhibited slightly redshifted absorption peaks and similar energy levels in comparison to that of the symmetric one, with optical gaps at around 1.40 eV. The electron/hole mobilities of the blend films with PM6 as the donor polymer were  $2.19 \times 10^{-4}/3.30 \times 10^{-4} \text{ cm}^2 \text{ V}^{-1} \text{ s}^{-1}$ ,  $3.56 \times 10^{-4}/4.57 \times 10^{-4} \text{ cm}^2 \text{ V}^{-1} \text{ s}^{-1}$ ,  $3.74 \times 10^{-4}/4.71 \times 10^{-4} \text{ cm}^2 \text{ V}^{-1} \text{ s}^{-1}$ , and  $3.08 \times 10^{-4}/3.98 \times 10^{-4} \text{ cm}^2 \text{ V}^{-1} \text{ s}^{-1}$  for DPBDT-4Cl, POBDT-4Cl, COBDT-4Cl, and TOBDT, respectively. All the devices based on the four acceptors showed PCEs over 11%, and the best performing was shown by COBDT-4Cl, in accordance with enhanced molecular packing and crystallinity. It is noteworthy that DPBDT-4Cl is highly hindered. Reducing the steric hindrance by replacing one phenylhexyl side chain by an octyloxy one contributed to improving the photovoltaic parameters (see Table 2, entries 1, 2). Replacing the second phenylhexyl by an alkylthiophene did not cause improvement (see Table 2, entries 2, 4). Substituting the BDT core by the less hindered alkyl and alkoxy side chains led to the best OPV performances (see Table 2, entries 3). Unfortunately, the authors have not yet published results obtained from dialkyl- or dialkoxy-substituted symmetrical derivatives for comparison.
- Working on wide-bandgap molecules with an IT core end-capped with 1,3-diethyl-2-thioxodihydropyrimidine-4,6(1*H*,5*H*)-dione terminal groups, named as 2C6-IDTT-T and C6-IDTT-T, respectively, Xia and collaborators introduced asymmetry at the level of the thienothiophene parts of the molecule core: while the first one had two symmetric *n*-hexyl chains, the second one exhibited asymmetric structure after removing of one of the *n*-hexyl chains (see Figure 7, molecules 40, 41) [146]. Thin films of the asymmetric compound exhibited greater redshift absorption than that of the symmetric one, that was attributed to efficient  $\pi$ - $\pi$  intermolecular interactions in the solid state. The optimized asymmetric C6-IDTT-T-based device afforded a PCE of 8.51%, about 1% higher than that of the symmetric 2C6-IDTT-T (see Table 2, entries 5, 6). This has been related to higher electron mobility and more balanced charge carrier transport as well as to weaker bimolecular recombination and a more pronounced face-on orientation in the PTB7-Th blend films for C6-IDTT-T-based devices.

### 3.2.2. Introducing Asymmetry via Lateral Side Chains

- Since these first works on A-D-A'-D-A molecules, tremendous efforts have been made to obtain more efficient Y6 derivatives [132,147], the current goal being to achieve PCEs beyond 18%. Recently, new molecules were synthesized and studied, with linear and branched alkyl side chains introduced on the  $\alpha$ - or  $\beta$ -position of a pendant thiophene, with this alkylthiophenyl part being used in place of the *n*-undecyl linear

chain of Y6 (see Figure 7, molecules 44–46) [82]. The influence of isomerization of the alkyl side chains, *n*-octyl or 2-ethylhexyl, and of their position on the pendant thiophene was examined. No significant impact on the energetic parameters ( $E_g$  and HOMO/LUMO levels) was noted. However, the shape and substitution position of alkyl side chains greatly affected photovoltaic parameters of blends obtained by mixing the molecules with D18-Cl as the donor polymer. The D18-Cl:BTP-4F-T3EH blend, based on the molecule with 2-ethylhexyl chains introduced in the  $\beta$ - position, displayed the greatest PCE value of 18.25% whereas the D18-Cl:BTP-4F-T2C8 blend, based on the molecule with *n*-octyl chains introduced in the  $\alpha$ -position, exhibited the lowest PCE value of 15.92% (see Table 2, entries 10–12). This was in agreement with the SCLC charge mobilities measured on blends, which were  $\mu_e/\mu_h = 1.85 \times 10^{-4}/1.67 \times 10^{-4}$ ,  $2.0 \times 10^{-4}/1.69 \times 10^{-4}$ , and  $2.77 \times 10^{-4}/2.82 \times 10^{-4} \text{ cm}^2 \text{ V}^{-1} \text{ s}^{-1}$  for D18-Cl: BTP-4F-T2C8, D18-Cl: BTP-4F-T2EH, and D18-Cl: BTP-4F-T3EH, respectively. It could be seen by GIWAXS investigations that D18-Cl: BTP-4F-T3EH exhibited the strongest material crystallinity with a predominant face-on orientation.

- As for ITIC derivatives, a promising strategy is to introduce asymmetry via grafting different alkyl chains on the pyrroles or on the thiophenes of the central core of Y6 (see Figure 8, molecules 47–54), with resulting PCEs approaching 18.5%, as reported in Table 2, entries 13–21 [148–150]. In a recent work, Luo and collaborators compared results obtained with the symmetrical molecules Y6 and BTP-PhC6 (Figure 7, molecule 47) to those obtained from their asymmetrical counterpart BTP-PhC6-C11 (Figure 7, molecule 48) [149]. BTP-PhC6 was obtained by replacing the *n*-undecyl chains of Y6 by *meta*-hexylphenyl substituents. Interestingly, the three molecules afforded single crystals, which allowed comparative crystallographic analyses to probe the effect of asymmetry on packing. The smallest S...O distance was found for BTP-PhC6-C11, indicating a favored molecular packing. Four kinds of dimers involving different  $\pi \cdots \pi$  stacking effects were identified. By comparing the  $\pi \cdots \pi$  stacking distances of the corresponding dimers for the three molecules, it was observed that BTP-PhC6-C11 presented the strongest intermolecular interactions. This, together with hydrogen bonding interaction of C–H...O provided by the *meta*-hexylphenyl chain led to the tightest molecular packing for BTP-PhC6-C11, as confirmed by 2D GIWAXS measurements on neat films and in accordance with the largest  $\mu_e$  value measured for BTP-PhC6-C11 ( $8.22 \times 10^{-4} \text{ cm}^2 \text{ V}^{-1} \text{ s}^{-1}$  compared to  $5.51 \times 10^{-4} \text{ cm}^2 \text{ V}^{-1} \text{ s}^{-1}$  for Y6 and  $6.49 \times 10^{-4} \text{ cm}^2 \text{ V}^{-1} \text{ s}^{-1}$  for BTP-PhC6-C11). After blending with PM1 as the donor polymer, the photovoltaic parameters were measured, revealing an increase in  $V_{OC}$  and PCE with the increase in phenyl rings per molecule (see Table 2, entries 13–15), resulting in the highest value of PCE (18.33%) for the PM1:BTP-PhC6-C11.
- In the same spirit, but using other bulky side chains, Xiao and collaborators synthesized and studied the Y-C10ch molecule, bearing two 10-cyclohexyldecyl chains on the thiophene in place of the C11 chains of Y6 and the asymmetrical derivative A-C10ch where one 10-cyclohexyldecyl chain was replaced by a 2-butyloctyl branched chain (see Figure 7, molecules 50, 51) [151]. The data obtained with these molecules were compared to those offered by the previously described L8-BO (see Figure 8, molecule 49) [151]. Crystallographic analyses revealed different 3D network packing patterns for L8-BO in comparison to the two others since the 10-cyclohexyldecyl chains underwent a reinforcement in skeleton planarity, leading to a more compact molecular packing. Contrarily to the preceding example, mixed effects on the photovoltaic parameters were observed: the device based on Y-C10ch afforded the highest  $J_{SC}$  value ( $26.9 \text{ mA cm}^{-2}$  vs.  $25.6$  and  $26.5 \text{ mA cm}^{-2}$  for L8-BO and A-C10ch, respectively), while the device based on L8-BO delivered the highest  $V_{OC}/FF$  values ( $0.899 \text{ V}/78.8\%$  vs.  $0.858 \text{ V}/76.3\%$  and  $0.887 \text{ V}/78.1\%$  for Y-C10ch and A-C10ch, respectively). Finally, the best PCE of 18.4% was obtained with the PM6:A-C10ch blend (see Table 2, entries 16–18).



- Chen and collaborators recently proposed to apply a slight change to the Y6 molecular structure by replacing the ethylhexyl chains grafted on the pyrrole rings by other branched chains (Figure 7, molecules 52–54) [148]. The first observed effect using the bulkiest butyloctyl chains was higher and more balanced electron and hole mobilities ( $\mu_e/\mu_h = 1.98 \times 10^{-3}/1.34 \times 10^{-3} \text{ cm}^2 \text{ V}^{-1} \text{ s}^{-1}$  for PM6:BO-4F) than those of devices based on Y6 ( $\mu_e/\mu_h = 5.90 \times 10^{-4}/2.00 \times 10^{-4} \text{ cm}^2 \text{ V}^{-1} \text{ s}^{-1}$  for PM6:Y6 [69]). This effect was further enhanced by introducing asymmetry using ethylhexyl and hexyldecyl bulky branched chains ( $\mu_e/\mu_h = 1.73 \times 10^{-3}/2.36 \times 10^{-3} \text{ cm}^2 \text{ V}^{-1} \text{ s}^{-1}$  for PM6:EH-HD-4F). GIWAXS analyses demonstrated better molecular stacking for PM6:EH-HD-4F which also exhibited the highest crystal coherence length (of 24.33 Å vs. 23.02 Å and 21.69 Å for PM6:BO-4F and PM6:Bu-OD-4F, respectively), with all the blend films displaying preferential face-on orientation. As can be seen in Table 2, entries 19–21, asymmetry preferentially impacted the  $J_{SC}$  and FF values, with more favorable values for the PM6:EH-HD-4F blend with the best PCE of 18.34%. It can be noted, however, that the asymmetry is a sensitive parameter since in the case of Bu-OD-4F with 2-butyl and 2-octyldecyl side chains, the PCE value obtained (17.10%) was the lowest of the series, explained by a lower miscibility in the blend film compared to the other blends under study.

### 3.2.3. Introducing Asymmetry via Terminal Chains

- A few years ago, Ryu and collaborators introduced asymmetry by adding terminal octyl chains to the IDIC molecule. Depending on whether the additional chain was in position 6 or 5 of 2-(2,3-dihydro-3-oxo-1H-inden-1-ylidene) propanedinitrile (INCN) terminal moieties, they obtained the molecules IDICO1 and IDICO2 (see Figure 7, molecules 55, 56) [152]. As expected, the terminal octyl chains improved the solubility of the new molecules, but they also gave rise to greater miscibility with the donor polymer PBDB-T. Analyses of PBDB-T:IDIC, PBDB-T:IDICO1, and PBDB-T:IDICO2 blends by GIWAXS established a face-on-dominated orientation for the three blends, with a decreasing  $\pi$ - $\pi$  stacking distance of 3.99, 3.80, and 3.74/3.52 Å for PBDB-T:IDIC, PBDB-T:IDICO1, and PBDB-T:IDICO2, respectively, indicating a densely packed structure resulting from the presence of the terminal octyl chain as well as a significant influence of its location on the INCN moiety. The acceptor molecular structure also demonstrated a substantial influence on the photovoltaic performances of the resulting devices since IDICO1- and IDICO2-based devices exhibited improvements in both the open-circuit voltage and short-circuit current density, compared to those of the reference PBDB-T:IDIC device (see Table 2, entries 22–24). It is worth noting, however, that the asymmetry introduced via terminal chains is a sensitive parameter since in the case of the PBDB-T:IDICO2 blend, which exhibited the most dense packing mode, the best PCE value obtained (17.62%) was lower than that obtained with the PBDB-T:IDICO1 blend (19.83%). This study confirmed the sensitivity of active molecules to the presence of alkyl chains as structuring agents. In the PBDB-T:IDIC series, we can also mention the work of Li and collaborators who demonstrated that intercalation of a phenyl ring between the molecular backbone and the central hexyl chains or replacing the hexyl chains by phenylbutyl moieties resulted in totally changed photovoltaic performances [153]. They thus synthesized IDIC-Ph-C6 and IDIC-C4Ph (see Figure 7, molecules 57, 58) and compared the performances of their blends with the donor polymer PBDB-T to those obtained with the PBDB-T:IDIC mixture. Whereas the acceptor molecules presented similar HOMO/LUMO energy levels, their behaviors in blends were inversely disturbed by the presence and location of the phenyl ring: while the PBDB-T:IDIC blend presented a fairly well-balanced hole/electron mobility ratio ( $\mu_h/\mu_e = 0.834$ ), this ratio was totally unbalanced for PBDB-T:IDIC-PhC6 ( $\mu_h/\mu_e = 115.5$ ) and improved for PBDB-T:IDIC-C4Ph ( $\mu_h/\mu_e = 0.961$ ) with doubled values of hole and electron mobility (see Table 2, entries 25–27). Consequently, PBDB-

T:IDIC-PhC6-based devices presented low photovoltaic performances whereas better numbers were obtained from PBDB-T:IDIC-C4Ph-based devices.

**Table 2.** Photovoltaic performances of NFAs <sup>a</sup>.

Entry	Active Layer	Solvent	Additional Conditions	$\mu\text{h}/\mu\text{e}^{\text{b}}$ $10^{-4} \text{ cm}^2$ $\text{V}^{-1} \text{ s}^{-1}$	$V_{\text{OC}}^{\text{c}}$ (V)	$J_{\text{SC}}^{\text{c}}$ (mA $\text{cm}^{-2}$ )	FF <sup>c</sup> (%)	PCE <sup>c</sup> (%)	Ref.
1	PM6:DPBDT-4Cl	CF	TA 100 °C 10 min <sub>d</sub>	3.30/2.19	0.89	18.7	65	11.2	[144]
2	PM6:POBDT-4Cl	CF	TA 100 °C 10 min	4.57/3.56	0.87	20.7	67	12.3	[144]
3	PM6:COBDT-4Cl	CF	TA 100 °C 10 min	4.71/3.74	0.86	21.6	70	13.2	[144]
4	PM6:TOBDT	CF	-	3.98/3.08	0.88	18.3	67	11.0	[145]
5	PTB7-Th:2C6-IDTT-T	CF	0.3 vol% DIO	3.77/0.42	1.069	13.32	52.8	7.52	[146]
6	PTB7-Th:C6-IDTT-T	CF	0.4 vol% DIO	3.93/0.8	1.052	14.42	56.1	8.51	[146]
7	PBDB-T:Y5	CF	TA 100 °C 10 min	3.17/3.98	0.88	22.8	70.2	14.1	[141]
8	PM6:Y6	CF	TA 110 °C 10 min	2.00/5.90	0.83	25.3	74.8	15.7	[69]
9	PBDB-T-2F:BT-BO-4F	CF	-	18.36/8.42	0.83	28.4	70.3	16.6	[142]
10	D18-Cl:BTP-4F-T2C8	CF	SVA: CF 5 min <sup>e</sup>	1.67/1.85	0.880	24.56	73.59	15.92	[82]
11	D18-Cl:BTP-4F-T2EH	CF	SVA: CF 5 min	1.69/2.02	0.891	25.68	76.11	17.41	[82]
12	D18-Cl:BTP-4F-T3EH	CF	SVA: CF 5 min	2.82/2.77	0.873	26.84	77.85	18.25	[82]
13	PM1:Y6	CF	TA 100 °C 5 min	3.29/4.12	0.864	26.07	75.77	17.06	[149]
14	PM1:BTP-PhC6	CF	TA 100 °C 5 min	4.58/5.38	0.884	25.30	77.86	17.43	[149]
15	PM1:BTP-PhC6-C11	CF	TA 100 °C 5 min	6.67/6.83	0.871	26.62	79.05	18.33	[149]
16	PM6:L8-BO	CF	-	5.70/3.90	0.899	25.6	78.8	18.1	[150]
17	PM6:Y-C10ch	CF	-	5.91/4.02	0.858	26.9	76.3	17.6	[150]
18	PM6:A-C10ch	CF	-	5.28/3.81	0.887	26.5	78.1	18.4	[150]
19	PM6:BO-4F	ClBz	TA 100 °C 10 min	13.4/19.8	0.84	27.0	76.7	17.39	[148]
20	PM6:Bu-OD-4F	ClBz	TA 100 °C 10 min	20.1/8.5	0.85	26.2	76.6	17.10	[148]
21	PM6:EH-HD-4F	ClBz	TA 100 °C 10 min	23.6/17.3	0.84	27.5	79.3	18.34	[148]
22	PBDB-T:IDIC	diClBz	-	2.27/0.352	0.67	0.074	57	10.08	[152]
23	PBDB-T:IDICO1	diClBz	-	2.02/0.45	0.76	0.121	61	19.83	[152]
24	PBDB-T:IDICO2	diClBz	-	1.28/0.237	0.74	0.113	59	17.62	[152]
25	PBDB-T:IDIC	ClBz	TA 130 °C 5 min	2.42/2.90	0.819	17.27	73.6	10.41	[153]
26	PBDB-T:IDIC-Ph-C6	ClBz	TA 130 °C 5 min	2.31/0.02	0.869	12.20	57.90	6.14	[153]
27	PBDB-T:IDIC-C4Ph	ClBz	TA 130 °C 5 min	4.70/4.89	0.822	18.08	77.42	11.50	[153]

<sup>a</sup> Structures of NFAs are provided in Figure 7. <sup>b</sup> Blend charge mobilities. <sup>c</sup> Data of the best performances when reported; otherwise, average values. <sup>d</sup> TA: thermal annealing. <sup>e</sup> SVA: solvent annealing. DCM: dichloromethane, CF: chloroform, ClBz: chlorobenzene, diClBz: o-dichlorobenzene, THF: tetrahydrofuran, CM: chloromethane, CS<sub>2</sub>: carbon disulfide. DIO: additive 1,8-diiodooctane.

### 3.2.4. Machine Learning

The collection of data for analyzing published results and comprehending experimental and fundamental aspects that govern the performance of materials for OPVs is a growing field known as machine learning. Combining machine learning and DFT calculations can be used for imaging new molecules to be synthesized [154]. Zhang and collaborators recently proposed a screening of Y6-based symmetric molecules via a machine learning model, based on collected performance data of all-organic solar cells employing Y6 and its derivatives as acceptor materials from the literature [155]. The aim was to obtain potential OPV molecules with high performance in order to save resources and accelerate the development of new OPV materials. As part of their work, they have explored the role of linear or branched alkyl chains grafted on the pyrrole and thiophene parts of the central core of the Y6 molecule. Interestingly, they obtained predicted PCEs greater than 17% for twenty-three virtual structures, three of them having already been described with measured PCE values between 17.39 and 18.32%, demonstrating the good predictive ability of their machine learning model. This work thus opens the way to new approaches for designing novel and promising OPV molecules.

## 4. Summary and Outlook

From initially solubilizing agents, alkyl side chains quickly became key tools in the engineering of organic materials for OPVs, polymers, and small molecules, and are now well recognized to be of great importance in the photovoltaic performance of devices.

Using alkyl chains in modulating their length, branched or linear character, and position of grafting onto the polymer or small molecule is a promising way for obtaining appropriate morphologies, while they often have a minor impact on the energetic parameters of the materials in solution. Peripheral linear chains sometimes help in reinforcing aggregation. If this effect is well controlled, it may lead to quite ideal morphology, and even to a liquid crystal state that has been proved to be beneficial for material structuration and enhanced photovoltaic parameters. On the contrary, a too-reinforced aggregation may provoke subsequent D/A demixing which is detrimental for morphology stability. Branched chains are good agents for disrupting initial strong  $\pi$ - $\pi$  stacking of polymers or small molecules. The selected examples discussed in this review show how fine-tuning can be reached even with methyl as the short chain, and how thin the frontiers are between too-aggregated, completely disorganized, and ideally arranged organic phases. They also show that there is no direct law for building ideal new materials. Even if the considerable efforts of researchers result in excellent results with PCEs approaching 19%, there is still a lot of investigation to be carried out on the correlation between molecular structure and the packing modes in blends.

Exploring the potential of new organic materials relies on accessing a large library of polymers and small molecules, but this supposes limitations linked to the synthesis workload are overcome. Currently, most of the new materials are generated one by one, in various quantities and using different purification techniques that require great synthesis expertise. The need for new techniques allowing high productivity, time and reagent saving, as well as excellent reproducibility is becoming crucial. A solution was proposed in 2015 by Li and collaborators who described the synthesis of a large library of building-block-based small molecules using an automated process [156]. Continued progress in this direction has been recently reviewed [157], and a recent paper exemplifies the use of automated synthesis for obtaining a library of conjugated oligomers with systematically varied side chain composition [158]. Such innovative solutions could be exploited to overcome synthesis issues.

In this paper, we reviewed recent papers dealing with polymer and molecule engineering using alkyl chains as key parameters for blend morphology optimization. The approach adopted is often empirical and consists in using a promising  $\pi$ -conjugated structure offering optimized electronic parameters and then introducing in its central, lateral, or terminal position linear or branched alkyl chains in order to observe the impact of these chains on molecular organization in bulk. Even if this strategy may lead to improved OPV parameters, it is time and money consuming. As discussed in Section 3.2.4, one solution to improve efficiency and scientific rationalization could be computational approaches. They are currently emerging for helping the chemist community in molecular design using screening calculations and machine learning [159–164]. They are based on experimental data that are still not extensively available. However, in gradually completing the databases, the scientific community will rapidly have the means to make increasingly reliable modeling chain conformations and bulk morphology.

In another way, and in the majority of cases, current research is essentially turned towards the synthesis and investigation of a champion polymer or molecule. When the latter is a donor (or an acceptor), a series of parent materials are synthesized and generally all tested with a common acceptor (or donor) material. This strategy therefore consists of independently optimizing one class of material. There should be growing impetus for this strategy to evolve through simultaneous and joint molecular engineering of both donor/acceptor materials, in order to multiply the number of promising D/A pairs.

Besides the work on molecular engineering, a concern about the impact of the nature of the alkyl chains on the chemical stability of organic materials for OPV cells could arise. However, it is hazardous to consider each component independently because the materials constituting the active layer are intimately mixed and cannot separate without special waste treatment. In a recent paper dealing with the stability of large-area OPV cells, Park and collaborators pointed out that despite the numerous studies devoted to degradation

mechanisms, the stability/degradation issue remains difficult to rationalize because of the various chemical, photochemical, and thermal ways organic materials degrade [165]. The degradation mechanisms are linked to different sources: the chemical structures of organic materials, the processing (coating) techniques, the nature of the charge-transporting interlayers. Moreover, indoor conditions for the study of degradation are often preferred because “data collection time is shortened and the degradation factors can be well controlled and defined”, but they are difficult to extrapolate to real outdoor environments. Thus, in these conditions, it is difficult to anticipate the impact of the nature and length of alkyl chains attached to organic polymers and small molecules on their degradation.

In summary, the grafting of alkyl side chains of different natures and lengths onto organic materials has turned OPV research from solving solubility issues into a promising control of the morphology of mixtures. Thanks to the progress in fundamental organic and materials chemistry, organic materials can be modified to improve the active layer efficiency. Following the design strategies discussed above, as well as new strategies to be developed further, we believe that new materials will be generated and even higher device performances will be achieved. We hope that a more comprehensive understanding on the structure–property–processing relationship of organic materials for OPVs will be accomplished and will impact other fields of organic electronics, flexible organic electronic devices, organic thin film transistors (OTFTs), UV–Vis and ionizing radiation detectors, memories, and chemical and biological sensors.

**Funding:** This research received no external funding.

**Conflicts of Interest:** The author declares no conflict of interest.

## References

1. Solak, E.K.; Irmak, E. Advances in Organic Photovoltaic Cells: A Comprehensive Review of Materials, Technologies, and Performance. *RSC Adv.* **2023**, *13*, 12244–12269. [[CrossRef](#)] [[PubMed](#)]
2. Zhou, Y.; Luo, X.; Yang, J.; Qiu, Q.; Xie, T.; Liang, T. Application of Quantum Dot Interface Modification Layer in Perovskite Solar Cells: Progress and Perspectives. *Nanomaterials* **2022**, *12*, 2102. [[CrossRef](#)] [[PubMed](#)]
3. Arzhanov, A.I.; Savostianov, A.O.; Magaryan, K.A.; Karimullin, K.R.; Naumov, A.V. Photonics of Semiconductor Quantum Dots: Applied Aspects. *Photonics Russ.* **2022**, *16*, 96–112. [[CrossRef](#)]
4. Chen, Y.; Sun, Y.; Peng, J.; Zhang, W.; Su, X.; Zheng, K.; Pullerits, T.; Liang, Z. Tailoring Organic Cation of 2D Air-Stable Organometal Halide Perovskites for Highly Efficient Planar Solar Cells. *Adv. Energy Mater.* **2017**, *7*, 1700162. [[CrossRef](#)]
5. Li, F.; Xie, Y.; Hu, Y.; Long, M.; Zhang, Y.; Xu, J.; Qin, M.; Lu, X.; Liu, M. Effects of Alkyl Chain Length on Crystal Growth and Oxidation Process of Two-Dimensional Tin Halide Perovskites. *ACS Energy Lett.* **2020**, *5*, 1422–1429. [[CrossRef](#)]
6. Tang, C.W. Two-layer Organic Photovoltaic Cell. *Appl. Phys. Lett.* **1986**, *48*, 183–185. [[CrossRef](#)]
7. Luo, D.; Jang, W.; Babu, D.D.; Kim, M.S.; Wang, D.H.; Kyaw, A.K.K. Recent Progress in Organic Solar Cells Based on Non-Fullerene Acceptors: Materials to Devices. *J. Mater. Chem. A* **2022**, *10*, 3255–3295. [[CrossRef](#)]
8. Ng, L.W.T.; Lee, S.W.; Chang, D.W.; Hodgkiss, J.M.; Vak, D. Organic Photovoltaics’ New Renaissance: Advances Toward Roll-to-Roll Manufacturing of Non-Fullerene Acceptor Organic Photovoltaics. *Adv. Mater. Technol.* **2022**, *7*, 2101556. [[CrossRef](#)]
9. Soonmin, H.; Hardani; Nandi, P.; Mwankemwa, B.S.; Malevu, T.D.; Malik, M.I. Overview on Different Types of Solar Cells: An Update. *Appl. Sci.* **2023**, *13*, 2051. [[CrossRef](#)]
10. Yu, G.; Gao, J.; Hummelen, J.C.; Wudl, F.; Heeger, A.J. Polymer Photovoltaic Cells: Enhanced Efficiencies via a Network of Internal Donor–Acceptor Heterojunctions. *Science* **1995**, *270*, 1789–1791. [[CrossRef](#)]
11. Peumans, P.; Uchida, S.; Forrest, S.R. Efficient Bulk Heterojunction Photovoltaic Cells Using Small-Molecular-Weight Organic Thin Films. *Nature* **2003**, *425*, 158–162. [[CrossRef](#)]
12. Clarke, T.M.; Durrant, J.R. Charge Photogeneration in Organic Solar Cells. *Chem. Rev.* **2010**, *110*, 6736–6767. [[CrossRef](#)] [[PubMed](#)]
13. Bredas, J.-L. Molecular Understanding of Organic Solar Cells: The Challenges. *AIP Conf. Proc.* **2013**, *1519*, 55–58. [[CrossRef](#)]
14. Wan, X.; Li, C.; Zhang, M.; Chen, Y. Acceptor–Donor–Acceptor Type Molecules for High Performance Organic Photovoltaics—Chemistry and Mechanism. *Chem. Soc. Rev.* **2020**, *49*, 2828–2842. [[CrossRef](#)] [[PubMed](#)]
15. Yue, Q.; Liu, W.; Zhu, X. N-Type Molecular Photovoltaic Materials: Design Strategies and Device Applications. *J. Am. Chem. Soc.* **2020**, *142*, 11613–11628. [[CrossRef](#)]
16. Cheng, P.; Yang, Y. Narrowing the Band Gap: The Key to High-Performance Organic Photovoltaics. *Acc. Chem. Res.* **2020**, *53*, 1218–1228. [[CrossRef](#)]
17. Ramirez, I.; Causa, M.; Zhong, Y.; Banerji, N.; Riede, M. Key Tradeoffs Limiting the Performance of Organic Photovoltaics. *Adv. Energy Mater.* **2018**, *8*, 1703551. [[CrossRef](#)]

18. Saito, M.; Ohkita, H.; Osaka, I.  $\pi$ -Conjugated Polymers and Molecules Enabling Small Photon Energy Loss Simultaneously with High Efficiency in Organic Photovoltaics. *J. Mater. Chem. A* **2020**, *8*, 20213–20237. [[CrossRef](#)]
19. Zhang, Y.; Duan, C.; Ding, L. Indoor Organic Photovoltaics. *Sci. Bull.* **2020**, *65*, 2040–2042. [[CrossRef](#)]
20. Ostroverkhova, O. Organic Optoelectronic Materials: Mechanisms and Applications. *Chem. Rev.* **2016**, *116*, 13279–13412. [[CrossRef](#)]
21. Zhang, G.; Zhao, J.; Chow, P.C.Y.; Jiang, K.; Zhang, J.; Zhu, Z.; Zhang, J.; Huang, F.; Yan, H. Nonfullerene Acceptor Molecules for Bulk Heterojunction Organic Solar Cells. *Chem. Rev.* **2018**, *118*, 3447–3507. [[CrossRef](#)] [[PubMed](#)]
22. Huang, W.; Cheng, P.; Yang, Y.M.; Li, G.; Yang, Y. High-Performance Organic Bulk-Heterojunction Solar Cells Based on Multiple-Donor or Multiple-Acceptor Components. *Adv. Mater.* **2018**, *30*, 1705706. [[CrossRef](#)] [[PubMed](#)]
23. Ilmi, R.; Haque, A.; Khan, M.S. High Efficiency Small Molecule-Based Donor Materials for Organic Solar Cells. *Org. Electron.* **2018**, *58*, 53–62. [[CrossRef](#)]
24. Li, T.; Chen, Z.; Wang, Y.; Tu, J.; Deng, X.; Li, Q.; Li, Z. Materials for Interfaces in Organic Solar Cells and Photodetectors. *ACS Appl. Mater. Interfaces* **2020**, *12*, 3301–3326. [[CrossRef](#)]
25. Jao, M.-H.; Liao, H.-C.; Su, W.-F. Achieving a High Fill Factor for Organic Solar Cells. *J. Mater. Chem. A* **2016**, *4*, 5784–5801. [[CrossRef](#)]
26. Li, S.; Ye, L.; Zhao, W.; Liu, X.; Zhu, J.; Ade, H.; Hou, J. Design of a New Small-Molecule Electron Acceptor Enables Efficient Polymer Solar Cells with High Fill Factor. *Adv. Mater.* **2017**, *29*, 1704051. [[CrossRef](#)]
27. Lin, Y.; Adilbekova, B.; Firdaus, Y.; Yengel, E.; Faber, H.; Sajjad, M.; Zheng, X.; Yarali, E.; Seitkhan, A.; Bakr, O.M.; et al. 17% Efficient Organic Solar Cells Based on Liquid Exfoliated WS<sub>2</sub> as a Replacement for PEDOT:PSS. *Adv. Mater.* **2019**, *31*, 1902965. [[CrossRef](#)]
28. Lin, Y.; Firdaus, Y.; Nugraha, M.I.; Liu, F.; Karuthedath, S.; Emwas, A.; Zhang, W.; Seitkhan, A.; Neophytou, M.; Faber, H.; et al. 17.1% Efficient Single-Junction Organic Solar Cells Enabled by N-Type Doping of the Bulk-Heterojunction. *Adv. Sci.* **2020**, *7*, 1903419. [[CrossRef](#)]
29. Cui, Y.; Yao, H.; Hong, L.; Zhang, T.; Tang, Y.; Lin, B.; Xian, K.; Gao, B.; An, C.; Bi, P.; et al. Organic photovoltaic cell with 17% efficiency and superior processability. *Natl. Sci. Rev.* **2020**, *7*, 1239–1246. [[CrossRef](#)]
30. Gao, H.; Sun, Y.; Meng, L.; Han, C.; Wan, X.; Chen, Y. Recent Progress in All-Small-Molecule Organic Solar Cells. *Small* **2023**, *19*, 2205594. [[CrossRef](#)]
31. Wen, Z.-C.; Yin, H.; Hao, X.-T. Recent Progress of PM6:Y6-Based High Efficiency Organic Solar Cells. *Surf. Interfaces* **2021**, *23*, 100921. [[CrossRef](#)]
32. Wang, X.; Sun, Q.; Gao, J.; Wang, J.; Xu, C.; Ma, X.; Zhang, F. Recent Progress of Organic Photovoltaics with Efficiency over 17%. *Energies* **2021**, *14*, 4200. [[CrossRef](#)]
33. Mohamed El Amine, B.; Zhou, Y.; Li, H.; Wang, Q.; Xi, J.; Zhao, C. Latest Updates of Single-Junction Organic Solar Cells up to 20% Efficiency. *Energies* **2023**, *16*, 3895. [[CrossRef](#)]
34. Wang, C.; Liu, Z.; Li, M.; Xie, Y.; Li, B.; Wang, S.; Xue, S.; Peng, Q.; Chen, B.; Zhao, Z.; et al. The Marriage of AIE and Interface Engineering: Convenient Synthesis and Enhanced Photovoltaic Performance. *Chem. Sci.* **2017**, *8*, 3750–3758. [[CrossRef](#)]
35. Goel, M.; Jayakannan, M. Supramolecular Liquid Crystalline  $\pi$ -Conjugates: The Role of Aromatic  $\pi$ -Stacking and van Der Waals Forces on the Molecular Self-Assembly of Oligophenylenevinylenes. *J. Phys. Chem. B* **2010**, *114*, 12508–12519. [[CrossRef](#)]
36. McCullough, R.D.; Lowe, R.D.; Jayaraman, M.; Anderson, D.L. Design, Synthesis, and Control of Conducting Polymer Architectures: Structurally Homogeneous Poly(3-Alkylthiophenes). *J. Org. Chem.* **1993**, *58*, 904–912. [[CrossRef](#)]
37. McCullough, R.D.; Tristram-Nagle, S.; Williams, S.P.; Lowe, R.D.; Jayaraman, M. Self-Orienting Head-to-Tail Poly(3-Alkylthiophenes): New Insights on Structure-Property Relationships in Conducting Polymers. *J. Am. Chem. Soc.* **1993**, *115*, 4910–4911. [[CrossRef](#)]
38. Chen, T.A.; Rieke, R.D. The First Regioregular Head-to-Tail Poly(3-Hexylthiophene-2,5-Diyl) and a Regiorandom Isopolymer: Nickel versus Palladium Catalysis of 2(5)-Bromo-5(2)-(Bromozincio)-3-Hexylthiophene Polymerization. *J. Am. Chem. Soc.* **1992**, *114*, 10087–10088. [[CrossRef](#)]
39. Sirringhaus, H. Integrated Optoelectronic Devices Based on Conjugated Polymers. *Science* **1998**, *280*, 1741–1744. [[CrossRef](#)]
40. Chirvase, D.; Chiguvare, Z.; Knipper, M.; Parisi, J.; Dyakonov, V.; Hummelen, J.C. Temperature Dependent Characteristics of Poly(3 Hexylthiophene)-Fullerene Based Heterojunction Organic Solar Cells. *J. Appl. Phys.* **2003**, *93*, 3376–3383. [[CrossRef](#)]
41. Chirvase, D.; Chiguvare, Z.; Knipper, M.; Parisi, J.; Dyakonov, V.; Hummelen, J.C. Electrical and Optical Design and Characterisation of Regioregular Poly(3-Hexylthiophene-2,5diyl)/Fullerene-Based Heterojunction Polymer Solar Cells. *Synth. Met.* **2003**, *138*, 299–304. [[CrossRef](#)]
42. Hernandez-Maldonado, D.; Ramos, B.; Villeneuve-Faure, C.; Bedel-Pereira, E.; Séguy, I.; Sournia-Saquet, A.; Alary, F.; Heully, J.L.; Moineau-Chane Ching, K.I. Chain Ordering of Regioregular Polythiophene Films through Blending with a Nickel Bisdithiolen Complex. *Appl. Phys. Lett.* **2014**, *104*, 103302. [[CrossRef](#)]
43. Villeneuve-Faure, C.; Le Borgne, D.; Bedel-Pereira, E.; Moineau Chane-Ching, K.I.; Hernandez-Maldonado, D.; Séguy, I. Cross Kelvin Force Microscopy and Conductive Atomic Force Microscopy Studies of Organic Bulk Heterojunction Blends for Local Morphology and Electrical Behavior Analysis. *J. Appl. Phys.* **2015**, *117*, 055501. [[CrossRef](#)]
44. Villeneuve-Faure, C.; Le Borgne, D.; Ventalon, V.; Seguy, I.; Moineau-Chane Ching, K.I.; Bedel-Pereira, E. Nanoscale Investigations on Interchain Organization in Thin Films of Polymer-Liquid Crystal Blend. *J. Chem. Phys.* **2017**, *147*, 014701. [[CrossRef](#)]

45. Kim, Y.; Park, H.; Abdilla, A.; Yun, H.; Han, J.; Stein, G.E.; Hawker, C.J.; Kim, B.J. Chain-Length-Dependent Self-Assembly Behaviors of Discrete Conjugated Oligo(3-Hexylthiophene). *Chem. Mater.* **2020**, *32*, 3597–3607. [[CrossRef](#)]
46. Mehmood, U.; Al-Ahmed, A.; Hussein, I.A. Review on Recent Advances in Polythiophene Based Photovoltaic Devices. *Renew. Sustain. Energy Rev.* **2016**, *57*, 550–561. [[CrossRef](#)]
47. Nielsen, C.B.; McCulloch, I. Recent Advances in Transistor Performance of Polythiophenes. *Prog. Polym. Sci.* **2013**, *38*, 2053–2069. [[CrossRef](#)]
48. Marrocchi, A.; Lanari, D.; Facchetti, A.; Vaccaro, L. Poly(3-Hexylthiophene): Synthetic Methodologies and Properties in Bulk Heterojunction Solar Cells. *Energy Environ. Sci.* **2012**, *5*, 8457. [[CrossRef](#)]
49. Rubio Arias, J.J.; Vieira Marques, M.d.F. Performance of Poly(3-Hexylthiophene) in Bulk Heterojunction Solar Cells: Influence of Polymer Size and Size Distribution. *React. Funct. Polym.* **2017**, *113*, 58–69. [[CrossRef](#)]
50. Mei, J.; Bao, Z. Side Chain Engineering in Solution-Processable Conjugated Polymers. *Chem. Mater.* **2014**, *26*, 604–615. [[CrossRef](#)]
51. Lei, T.; Wang, J.-Y.; Pei, J. Roles of Flexible Chains in Organic Semiconducting Materials. *Chem. Mater.* **2014**, *26*, 594–603. [[CrossRef](#)]
52. Liu, Z.; Zhang, G.; Zhang, D. Modification of Side Chains of Conjugated Molecules and Polymers for Charge Mobility Enhancement and Sensing Functionality. *Acc. Chem. Res.* **2018**, *51*, 1422–1432. [[CrossRef](#)] [[PubMed](#)]
53. Skotheim, T.A. (Ed.) *Handbook of Conducting Polymers, Volume 1*; Marcel Dekker: New York, NY, USA, 1986.
54. Schopp, N.; Brus, V.V. A Review on the Materials Science and Device Physics of Semitransparent Organic Photovoltaics. *Energies* **2022**, *15*, 4639. [[CrossRef](#)]
55. Zhang, X.; Huang, H. Polymer-Related Organic Photovoltaics. *Macromol. Rapid Commun.* **2022**, *43*, 2200770. [[CrossRef](#)]
56. Al-Azzawi, A.G.S.; Aziz, S.B.; Dannoun, E.M.A.; Iraqi, A.; Nofal, M.M.; Murad, A.R.; Hussein, A.M. A Mini Review on the Development of Conjugated Polymers: Steps towards the Commercialization of Organic Solar Cells. *Polymers* **2023**, *15*, 164. [[CrossRef](#)]
57. Qiu, B.; Lai, J.; Yuan, J.; Zou, Y.; Li, Y. Recent Research Progress in Random Copolymerization of Polymer Photovoltaic Materials for High-Performance Polymer Solar Cells. *Sol. RRL* **2023**, *7*, 2300146. [[CrossRef](#)]
58. Tetreault, A.R.; Dang, M.-T.; Bender, T.P. PTB7 and PTB7-Th as Universal Polymers to Evaluate Materials Development Aspects of Organic Solar Cells Including Interfacial Layers, New Fullerenes, and Non-Fullerene Electron Acceptors. *Synth. Met.* **2022**, *287*, 117088. [[CrossRef](#)]
59. Cong, P.; Wang, Z.; Geng, Y.; Meng, Y.; Meng, C.; Chen, L.; Tang, A.; Zhou, E. Benzothiadiazole-Based Polymer Donors. *Nano Energy* **2023**, *105*, 108017. [[CrossRef](#)]
60. An, C.; Hou, J. Benzo[1,2-b:4,5-b']Dithiophene-Based Conjugated Polymers for Highly Efficient Organic Photovoltaics. *Acc. Mater. Res.* **2022**, *3*, 540–551. [[CrossRef](#)]
61. Hacefendioglu, T.; Yildirim, E. Design Principles for the Acceptor Units in Donor-Acceptor Conjugated Polymers. *ACS Omega* **2022**, *7*, 38969–38978. [[CrossRef](#)]
62. Guo, Q.; Guo, Q.; Geng, Y.; Tang, A.; Zhang, M.; Du, M.; Sun, X.; Zhou, E. Recent Advances in PM6:Y6-Based Organic Solar Cells. *Mater. Chem. Front.* **2021**, *5*, 3257–3280. [[CrossRef](#)]
63. Kim, M.; Choi, Y.; Hwan Lee, D.; Min, J.; Pu, Y.-J.; Park, T. Roles and Impacts of Ancillary Materials for Multi-Component Blend Organic Photovoltaics towards High Efficiency and Stability. *ChemSusChem* **2021**, *14*, 3475–3487. [[CrossRef](#)] [[PubMed](#)]
64. Meng, D.; Zheng, R.; Zhao, Y.; Zhang, E.; Dou, L.; Yang, Y. Near-Infrared Materials: The Turning Point of Organic Photovoltaics. *Adv. Mater.* **2022**, *34*, 2107330. [[CrossRef](#)] [[PubMed](#)]
65. Wenderott, J.K.; Dong, B.X.; Green, P.F. Morphological Design Strategies to Tailor Out-of-Plane Charge Transport in Conjugated Polymer Systems for Device Applications. *Phys. Chem. Chem. Phys.* **2021**, *23*, 27076–27102. [[CrossRef](#)]
66. Liu, Q.; Jiang, Y.; Jin, K.; Qin, J.; Xu, J.; Li, W.; Xiong, J.; Liu, J.; Xiao, Z.; Sun, K.; et al. 18% Efficiency Organic Solar Cells. *Sci. Bull.* **2020**, *65*, 272–275. [[CrossRef](#)]
67. Zhu, L.; Zhang, M.; Xu, J.; Li, C.; Yan, J.; Zhou, G.; Zhong, W.; Hao, T.; Song, J.; Xue, X.; et al. Single-Junction Organic Solar Cells with over 19% Efficiency Enabled by a Refined Double-Fibril Network Morphology. *Nat. Mater.* **2022**, *21*, 656–663. [[CrossRef](#)]
68. Weng, K.; Ye, L.; Zhu, L.; Xu, J.; Zhou, J.; Feng, X.; Lu, G.; Tan, S.; Liu, F.; Sun, Y. Optimized Active Layer Morphology toward Efficient and Polymer Batch Insensitive Organic Solar Cells. *Nat. Commun.* **2020**, *11*, 2855. [[CrossRef](#)]
69. Yuan, J.; Zhang, Y.; Zhou, L.; Zhang, G.; Yip, H.-L.; Lau, T.-K.; Lu, X.; Zhu, C.; Peng, H.; Johnson, P.A.; et al. Single-Junction Organic Solar Cell with over 15% Efficiency Using Fused-Ring Acceptor with Electron-Deficient Core. *Joule* **2019**, *3*, 1140–1151. [[CrossRef](#)]
70. Li, N.; Perea, J.D.; Kassar, T.; Richter, M.; Heumueller, T.; Matt, G.J.; Hou, Y.; Güldal, N.S.; Chen, H.; Chen, S.; et al. Abnormal Strong Burn-in Degradation of Highly Efficient Polymer Solar Cells Caused by Spinodal Donor-Acceptor Demixing. *Nat. Commun.* **2017**, *8*, 14541. [[CrossRef](#)]
71. Tegegne, N.A.; Abdissa, Z.; Mammo, W.; Uchiyama, T.; Okada-Shudo, Y.; Galeotti, F.; Porzio, W.; Andersson, M.R.; Schlettwein, D.; Vohra, V.; et al. Effect of Alkyl Side Chain Length on Intra- and Intermolecular Interactions of Terthiophene-Isoindigo Copolymers. *J. Phys. Chem. C* **2020**, *124*, 9644–9655. [[CrossRef](#)]
72. Zhang, C.-H.; Lin, F.; Huang, W.; Xin, J.; Wang, J.; Lin, Z.; Ma, W.; Yang, T.; Xia, J.; Liang, Y. Methyl Functionalization on Conjugated Side Chains for Polymer Solar Cells Processed from Non-Chlorinated Solvents. *J. Mater. Chem. C Mater. Opt. Electron. Devices* **2020**, *8*, 11532–11539. [[CrossRef](#)]

73. Wu, Y.; Schneider, S.; Walter, C.; Chowdhury, A.H.; Bahrami, B.; Wu, H.-C.; Qiao, Q.; Toney, M.F.; Bao, Z. Fine-Tuning Semiconducting Polymer Self-Aggregation and Crystallinity Enables Optimal Morphology and High-Performance Printed All-Polymer Solar Cells. *J. Am. Chem. Soc.* **2020**, *142*, 392–406. [[CrossRef](#)] [[PubMed](#)]
74. Zhou, J.; Zhang, B.; Du, M.; Dai, T.; Tang, A.; Guo, Q.; Zhou, E. Side-Chain Engineering of Copolymers Based on Benzotriazole (BTA) and Dithieno[2,3-d;2'',3''-D'']Benzo[1,2-b;4,5-b'']Dithiophenes (DTBDT) Enables a High PCE of 14.6%. *Nanotechnology* **2021**, *32*, 225403. [[CrossRef](#)] [[PubMed](#)]
75. Chen, J.; Huang, X.; Cao, Z.; Liu, S.; Liang, K.; Liu, J.; Jiao, X.; Zhao, J.; Li, Q.; Cai, Y.-P. Pronounced Dependence of All-Polymer Solar Cells Photovoltaic Performance on the Alkyl Substituent Patterns in Large Bandgap Polymer Donors. *ChemPhysChem* **2020**, *21*, 908–915. [[CrossRef](#)]
76. Li, X.; Duan, X.; Qiao, J.; Li, S.; Cai, Y.; Zhang, J.; Zhang, Y.; Hao, X.; Sun, Y. Benzotriazole-Based Polymer Acceptor for High-Efficiency All-Polymer Solar Cells with High Photocurrent and Low Voltage Loss. *Adv. Energy Mater.* **2023**, *13*, 2203044. [[CrossRef](#)]
77. Costa, C.; Farinhas, J.; Galvao, A.M.; Charas, A. On the Effect of Pattern Substitution and Oligo(Ethylene Oxide) Side-Chain Modification on Thiophene-Quinoxaline Copolymers and Their Applications in Photovoltaic Cells. *Org. Electron.* **2020**, *78*, 105612. [[CrossRef](#)]
78. Kim, Y.; Yeom, H.R.; Kim, J.Y.; Yang, C. High-Efficiency Polymer Solar Cells with a Cost-Effective Quinoxaline Polymer through Nanoscale Morphology Control Induced by Practical Processing Additives. *Energy Environ. Sci.* **2013**, *6*, 1909. [[CrossRef](#)]
79. Sun, C.; Pan, F.; Qiu, B.; Qin, S.; Chen, S.; Shang, Z.; Meng, L.; Yang, C.; Li, Y. D-A Copolymer Donor Based on Bithienyl Benzodithiophene D-Unit and Monoalkoxy Bifluoroquinoxaline A-Unit for High-Performance Polymer Solar Cells. *Chem. Mater.* **2020**, *32*, 3254–3261. [[CrossRef](#)]
80. Zhu, C.; Meng, L.; Zhang, J.; Qin, S.; Lai, W.; Qiu, B.; Yuan, J.; Wan, Y.; Huang, W.; Li, Y. A Quinoxaline-Based D-A Copolymer Donor Achieving 17.62% Efficiency of Organic Solar Cells. *Adv. Mater.* **2021**, *33*, 2100474. [[CrossRef](#)]
81. Hou, J.; Park, M.-H.; Zhang, S.; Yao, Y.; Chen, L.-M.; Li, J.-H.; Yang, Y. Bandgap and Molecular Energy Level Control of Conjugated Polymer Photovoltaic Materials Based on Benzo[1,2-b:4,5-b']Dithiophene. *Macromolecules* **2008**, *41*, 6012–6018. [[CrossRef](#)]
82. Shang, A.; Luo, S.; Zhang, J.; Zhao, H.; Xia, X.; Pan, M.; Li, C.; Chen, Y.; Yi, J.; Lu, X.; et al. Over 18% Binary Organic Solar Cells Enabled by Isomerization of Non-Fullerene Acceptors with Alkylthiophene Side Chains. *Sci. China Chem.* **2022**, *65*, 1758–1766. [[CrossRef](#)]
83. Sun, L.; Fukuda, K.; Someya, T. Recent Progress in Solution-Processed Flexible Organic Photovoltaics. *Npj Flex. Electron.* **2022**, *6*, 89. [[CrossRef](#)]
84. Busireddy, M.R.; Chen, T.-W.; Huang, S.-C.; Su, Y.-J.; Wang, Y.-M.; Chuang, W.-T.; Chen, J.-T.; Hsu, C.-S. PBDB-T-Based Binary-OSCs Achieving over 15.83% Efficiency via End-Group Functionalization and Alkyl-Chain Engineering of Quinoxaline-Containing Non-Fullerene Acceptors. *ACS Appl. Mater. Interfaces* **2022**, *14*, 41264–41274. [[CrossRef](#)] [[PubMed](#)]
85. Bin, H.; Yang, Y.; Peng, Z.; Ye, L.; Yao, J.; Zhong, L.; Sun, C.; Gao, L.; Huang, H.; Li, X.; et al. Effect of Alkylsilyl Side-Chain Structure on Photovoltaic Properties of Conjugated Polymer Donors. *Adv. Energy Mater.* **2018**, *8*, 1702324. [[CrossRef](#)]
86. Yan, T.; Bin, H.; Sun, C.; Zhang, Z.-G.; Li, Y. Synthesis and Photovoltaic Properties of 2D-Conjugated Polymers with Alkylsilyl-Substituted Thieno[3,2-b]Thiophene Conjugated Side Chains. *Org. Electron.* **2018**, *57*, 255–262. [[CrossRef](#)]
87. Huang, B.; Chen, L.; Jin, X.; Chen, D.; An, Y.; Xie, Q.; Tan, Y.; Lei, H.; Chen, Y. Alkylsilyl Functionalized Copolymer Donor for Annealing-Free High Performance Solar Cells with over 11% Efficiency: Crystallinity Induced Small Driving Force. *Adv. Funct. Mater.* **2018**, *28*, 1800606. [[CrossRef](#)]
88. Huang, B.; Hu, L.; Chen, L.; Chen, S.; Hu, M.; Zhou, Y.; Zhang, Y.; Yang, C.; Chen, Y. Morphological Optimization by Rational Matching of the Donor and Acceptor Boosts the Efficiency of Alkylsilyl Fused Ring-Based Polymer Solar Cells. *J. Mater. Chem. Mater. Energy Sustain.* **2019**, *7*, 4847–4854. [[CrossRef](#)]
89. Bin, H.; Van Der Pol, T.P.A.; Li, J.; Van Gorkom, B.T.; Wienk, M.M.; Janssen, R.A.J. Efficient Organic Solar Cells with Small Energy Losses Based on a Wide-Bandgap Trialkylsilyl-Substituted Donor Polymer and a Non-Fullerene Acceptor. *Chem. Eng. J.* **2022**, *435*, 134878. [[CrossRef](#)]
90. Zhou, J.; Lei, P.; Geng, Y.; He, Z.; Li, X.; Zeng, Q.; Tang, A.; Zhou, E. A Linear 2D-Conjugated Polymer Based on 4,8-Bis(4-Chloro-5-Tripropylsilyl-Thiophen-2-Yl)Benzo[1,2-b:4,5-b']Dithiophene (BDT-T-SiCl) for Low Voltage Loss Organic Photovoltaics. *J. Mater. Chem. A* **2022**, *10*, 9869–9877. [[CrossRef](#)]
91. Genene, Z.; Negash, A.; Abdulahi, B.A.; Eachambadi, R.T.; Liu, Z.; Van den Brande, N.; D'Haen, J.; Wang, E.; Vandewal, K.; Maes, W.; et al. Comparative Study on the Effects of Alkylsilyl and Alkylthio Side Chains on the Performance of Fullerene and Non-Fullerene Polymer Solar Cells. *Org. Electron.* **2020**, *77*, 105572. [[CrossRef](#)]
92. Akkerman, H.B.; Mannsfeld, S.C.B.; Kaushik, A.P.; Verploegen, E.; Burnier, L.; Zoombelt, A.P.; Saathoff, J.D.; Hong, S.; Atahan-Evrenk, S.; Liu, X.; et al. Effects of Odd–Even Side Chain Length of Alkyl-Substituted Diphenylbithiophenes on First Monolayer Thin Film Packing Structure. *J. Am. Chem. Soc.* **2013**, *135*, 11006–11014. [[CrossRef](#)] [[PubMed](#)]
93. Kuznetsov, I.E.; Nikitenko, S.L.; Kuznetsov, P.M.; Dremova, N.N.; Troshin, P.A.; Akkuratov, A.V. Solubilizing Side Chain Engineering: Efficient Strategy to Improve the Photovoltaic Performance of Novel Benzodithiophene-Based (X-DADAD)n Conjugated Polymers. *Macromol. Rapid Commun.* **2020**, *41*, 2000430. [[CrossRef](#)] [[PubMed](#)]

94. Chang, Y.; Lau, T.-K.; Chow, P.C.Y.; Wu, N.; Su, D.; Zhang, W.; Meng, H.; Ma, C.; Liu, T.; Li, K.; et al. A 16.4% Efficiency Organic Photovoltaic Cell Enabled Using Two Donor Polymers with Their Side-Chains Oriented Differently by a Ternary Strategy. *J. Mater. Chem. Mater. Energy Sustain.* **2020**, *8*, 3676–3685. [[CrossRef](#)]
95. Qin, F.; Sun, L.; Chen, H.; Liu, Y.; Lu, X.; Wang, W.; Liu, T.; Dong, X.; Jiang, P.; Jiang, Y.; et al. 54 cm<sup>2</sup> Large-Area Flexible Organic Solar Modules with Efficiency Above 13%. *Adv. Mater.* **2021**, *33*, 2103017. [[CrossRef](#)] [[PubMed](#)]
96. An, C.; Xin, J.; Shi, L.; Ma, W.; Zhang, J.; Yao, H.; Li, S.; Hou, J. Enhanced Intermolecular Interactions to Improve Twisted Polymer Photovoltaic Performance. *Sci. China Chem.* **2019**, *62*, 370–377. [[CrossRef](#)]
97. Lv, Q.; An, C.; Zhang, T.; Zhou, P.; Hou, J. Effect of Alkyl Side Chains of Twisted Conjugated Polymer Donors on Photovoltaic Performance. *Polymer* **2021**, *218*, 123475. [[CrossRef](#)]
98. Sun, X.; Lv, J.; Zhang, C.; Wang, K.; Yang, C.; Hu, H.; Ouyang, X. Morphology Controlling of All-Small-Molecule Organic Solar Cells: From Donor Material Design to Device Engineering. *Sol. RRL* **2023**, *7*, 2300332. [[CrossRef](#)]
99. Zhou, J.; Zuo, Y.; Wan, X.; Long, G.; Zhang, Q.; Ni, W.; Liu, Y.; Li, Z.; He, G.; Li, C.; et al. Solution-Processed and High-Performance Organic Solar Cells Using Small Molecules with a Benzodithiophene Unit. *J. Am. Chem. Soc.* **2013**, *135*, 8484–8487. [[CrossRef](#)]
100. Duan, T.; Liang, R.-Z.; Fu, Y.; Chang, Y.; Kan, Z.; Zhong, C.; Xie, Z.; Yu, D. Branched versus Linear: Side-Chain Effect on Fluorinated Wide Bandgap Donors and Their Applications in Organic Solar Cells. *New J. Chem.* **2020**, *44*, 753–760. [[CrossRef](#)]
101. Liu, D.; Yang, L.; Wu, Y.; Wang, X.; Zeng, Y.; Han, G.; Yao, H.; Li, S.; Zhang, S.; Zhang, Y.; et al. Tunable Electron Donating and Accepting Properties Achieved by Modulating the Steric Hindrance of Side Chains in A-D-A Small-Molecule Photovoltaic Materials. *Chem. Mater.* **2018**, *30*, 619–628. [[CrossRef](#)]
102. Hopper, T.R.; Qian, D.; Yang, L.; Wang, X.; Zhou, K.; Kumar, R.; Ma, W.; He, C.; Hou, J.; Gao, F.; et al. Control of Donor-Acceptor Photophysics through Structural Modification of a “Twisting” Push-Pull Molecule. *Chem. Mater.* **2019**, *31*, 6860–6869. [[CrossRef](#)]
103. Wang, Y.; Fan, Q.; Wang, Y.; Fang, J.; Liu, Q.; Zhu, L.; Qiu, J.; Guo, X.; Liu, F.; Su, W.; et al. Modulating Crystallinity and Miscibility via Side-Chain Variation Enable High Performance All-Small-Molecule Organic Solar Cells. *Chin. J. Chem.* **2021**, *39*, 2147–2153. [[CrossRef](#)]
104. Qiu, B.; Chen, Z.; Qin, S.; Yao, J.; Huang, W.; Meng, L.; Zhu, H.; Yang, Y.; Zhang, Z.-G.; Li, Y. Highly Efficient All-Small-Molecule Organic Solar Cells with Appropriate Active Layer Morphology by Side Chain Engineering of Donor Molecules and Thermal Annealing. *Adv. Mater.* **2020**, *32*, 1908373. [[CrossRef](#)] [[PubMed](#)]
105. Ma, K.; Feng, W.; Liang, H.; Chen, H.; Wang, Y.; Wan, X.; Yao, Z.; Li, C.; Kan, B.; Chen, Y. Modulation of Alkyl Chain Length on the Thiazole Side Group Enables Over 17% Efficiency in All-Small-Molecule Organic Solar Cells. *Adv. Funct. Mater.* **2023**, *33*, 2214926. [[CrossRef](#)]
106. Wang, X.; Li, Z.; Zheng, X.; Xiao, C.; Hu, T.; Liao, Y.; Yang, R. High-Efficiency All-Small-Molecule Organic Solar Cells Based on New Molecule Donors with Conjugated Symmetric/Asymmetric Hybrid Cyclopentyl-Hexyl Side Chains. *Adv. Funct. Mater.* **2023**, *33*, 2300323. [[CrossRef](#)]
107. Chen, H.; Hu, D.; Yang, Q.; Gao, J.; Fu, J.; Yang, K.; He, H.; Chen, S.; Kan, Z.; Duan, T.; et al. All-Small-Molecule Organic Solar Cells with an Ordered Liquid Crystalline Donor. *Joule* **2019**, *3*, 3034–3047. [[CrossRef](#)]
108. Tang, H.; Chen, H.; Yan, C.; Huang, J.; Fong, P.W.K.; Lv, J.; Hu, D.; Singh, R.; Kumar, M.; Xiao, Z.; et al. Delicate Morphology Control Triggers 14.7% Efficiency All-Small-Molecule Organic Solar Cells. *Adv. Energy Mater.* **2020**, *10*, 2001076. [[CrossRef](#)]
109. Hu, D.; Yang, Q.; Chen, H.; Wobben, F.; Le Corre, V.M.; Singh, R.; Liu, T.; Ma, R.; Tang, H.; Koster, L.J.A.; et al. 15.34% Efficiency All-Small-Molecule Organic Solar Cells with an Improved Fill Factor Enabled by a Fullerene Additive. *Energy Environ. Sci.* **2020**, *13*, 2134–2141. [[CrossRef](#)]
110. Cui, C.; Guo, X.; Min, J.; Guo, B.; Cheng, X.; Zhang, M.; Brabec, C.J.; Li, Y. High-Performance Organic Solar Cells Based on a Small Molecule with Alkylthio-Thienyl-Conjugated Side Chains without Extra Treatments. *Adv. Mater.* **2015**, *27*, 7469–7475. [[CrossRef](#)]
111. Zou, Y.; Wu, Y.; Yang, H.; Dong, Y.; Cui, C.; Li, Y. The Effect of Alkylthio Side Chains in Oligothiophene-Based Donor Materials for Organic Solar Cells. *Mol. Syst. Des. Eng.* **2018**, *3*, 131–141. [[CrossRef](#)]
112. Li, Y.; Zhong, Y.; Wen, S.; Zhang, Y.; Yang, R. Terminal Group Modification of Alkylthio Substituted Small Molecule Donor Materials for Organic Solar Cells. *Dyes Pigments* **2019**, *171*, 107653. [[CrossRef](#)]
113. Duan, T.; Tang, H.; Liang, R.-Z.; Lv, J.; Kan, Z.; Singh, R.; Kumar, M.; Xiao, Z.; Lu, S.; Laquai, F. Terminal Group Engineering for Small-Molecule Donors Boosts the Performance of Nonfullerene Organic Solar Cells. *J. Mater. Chem. A* **2019**, *7*, 2541–2546. [[CrossRef](#)]
114. Shi, Y.; Yang, C.; Li, H.; Liu, L.; Zhou, R.; Zou, W.; Wang, Z.; Wu, Q.; Deng, D.; Zhang, J.; et al. A- $\pi$ -D- $\pi$ -A Small-Molecule Donors with Different End Alkyl Chains Obtain Different Morphologies in Organic Solar Cells. *Chin. Chem. Lett.* **2019**, *30*, 906–910. [[CrossRef](#)]
115. Li, H.; Wu, Q.; Zhou, R.; Shi, Y.; Yang, C.; Zhang, Y.; Zhang, J.; Zou, W.; Deng, D.; Lu, K.; et al. Liquid-Crystalline Small Molecules for Nonfullerene Solar Cells with High Fill Factors and Power Conversion Efficiencies. *Adv. Energy Mater.* **2019**, *9*, 1803175. [[CrossRef](#)]
116. Wu, Q.; Deng, D.; Zhou, R.; Zhang, J.; Zou, W.; Liu, L.; Wu, S.; Lu, K.; Wei, Z. Modulation of Donor Alkyl Terminal Chains with the Shifting Branching Point Leads to the Optimized Morphology and Efficient All-Small-Molecule Organic Solar Cells. *ACS Appl. Mater. Interfaces* **2020**, *12*, 25100–25107. [[CrossRef](#)]



117. Zhi, H.; Jiang, M.; Zhang, H.; An, Q.; Bai, H.; Jee, M.H.; Woo, H.Y.; Li, D.; Huang, X.; Wang, J. Isomeric Small Molecule Donor with Terminal Branching Position Directly Attached to the Backbone Enables Efficient All-Small-Molecule Organic Solar Cells with Excellent Stability. *Adv. Funct. Mater.* **2023**, *33*, 2300878. [[CrossRef](#)]
118. Dang, M.T.; Hirsch, L.; Wantz, G.; Wuest, J.D. Controlling the Morphology and Performance of Bulk Heterojunctions in Solar Cells. Lessons Learned from the Benchmark Poly(3-Hexylthiophene):[6,6]-Phenyl-C<sub>61</sub>-Butyric Acid Methyl Ester System. *Chem. Rev.* **2013**, *113*, 3734–3765. [[CrossRef](#)]
119. Dang, M.T.; Hirsch, L.; Wantz, G. P3HT:PCBM, Best Seller in Polymer Photovoltaic Research. *Adv. Mater.* **2011**, *23*, 3597–3602. [[CrossRef](#)]
120. Xiao, J.; Jia, X.; Duan, C.; Huang, F.; Yip, H.; Cao, Y. Surpassing 13% Efficiency for Polythiophene Organic Solar Cells Processed from Nonhalogenated Solvent. *Adv. Mater.* **2021**, *33*, 2008158. [[CrossRef](#)]
121. Chatterjee, S.; Jinnai, S.; Ie, Y. Nonfullerene Acceptors for P3HT-Based Organic Solar Cells. *J. Mater. Chem. A* **2021**, *9*, 18857–18886. [[CrossRef](#)]
122. Yang, C.; Yu, R.; Liu, C.; Li, H.; Zhang, S.; Hou, J. Achieving over 10% Efficiency in Poly(3-hexylthiophene)-Based Organic Solar Cells via Solid Additives. *ChemSusChem* **2021**, *14*, 3607–3613. [[CrossRef](#)]
123. Liu, F.; Hou, T.; Xu, X.; Sun, L.; Zhou, J.; Zhao, X.; Zhang, S. Recent Advances in Nonfullerene Acceptors for Organic Solar Cells. *Macromol. Rapid Commun.* **2018**, *39*, 1700555. [[CrossRef](#)]
124. Forti, G.; Nitti, A.; Osw, P.; Bianchi, G.; Po, R.; Pasini, D. Recent Advances in Non-Fullerene Acceptors of the IDIC/ITIC Families for Bulk-Heterojunction Organic Solar Cells. *Int. J. Mol. Sci.* **2020**, *21*, 8085. [[CrossRef](#)] [[PubMed](#)]
125. Kan, B.; Kan, Y.; Zuo, L.; Shi, X.; Gao, K. Recent Progress on All-small Molecule Organic Solar Cells Using Small-molecule Nonfullerene Acceptors. *InfoMat* **2021**, *3*, 175–200. [[CrossRef](#)]
126. Zhu, L.; Zhang, M.; Zhong, W.; Leng, S.; Zhou, G.; Zou, Y.; Su, X.; Ding, H.; Gu, P.; Liu, F.; et al. Progress and Prospects of the Morphology of Non-Fullerene Acceptor Based High-Efficiency Organic Solar Cells. *Energy Environ. Sci.* **2021**, *14*, 4341–4357. [[CrossRef](#)]
127. Schweda, B.; Reinfelds, M.; Hofstadler, P.; Trimmel, G.; Rath, T. Recent Progress in the Design of Fused-Ring Non-Fullerene Acceptors—Relations between Molecular Structure and Optical, Electronic, and Photovoltaic Properties. *ACS Appl. Energy Mater.* **2021**, *4*, 11899–11981. [[CrossRef](#)]
128. Suzuki, M.; Suzuki, K.; Won, T.; Yamada, H. Impact of Substituents on the Performance of Small-Molecule Semiconductors in Organic Photovoltaic Devices via Regulating Morphology. *J. Mater. Chem. C* **2022**, *10*, 1162–1195. [[CrossRef](#)]
129. Murugan, P.; Hu, T.; Hu, X.; Chen, Y. Fused Ring A–DA'D–A (Y-Series) Non-Fullerene Acceptors: Recent Developments and Design Strategies for Organic Photovoltaics. *J. Mater. Chem. A* **2022**, *10*, 17968–17987. [[CrossRef](#)]
130. He, Q.; Kafourou, P.; Hu, X.; Heeney, M. Development of Non-Fullerene Electron Acceptors for Efficient Organic Photovoltaics. *SN Appl. Sci.* **2022**, *4*, 247. [[CrossRef](#)]
131. Mola, G.T.; Ahmed, A.Y.A.; Ike, J.N.; Liu, M.; Hamed, M.S.G.; Zhang, Y. Engineering Non-Fullerene Acceptors as a Mechanism to Control Film Morphology and Energy Loss in Organic Solar Cells. *Energy Fuels* **2022**, *36*, 4691–4707. [[CrossRef](#)]
132. Luo, Z.; Xu, T.; Zhang, C.; Yang, C. Side-Chain Engineering of Nonfullerene Small-Molecule Acceptors for Organic Solar Cells. *Energy Environ. Sci.* **2023**, *16*, 2732–2758. [[CrossRef](#)]
133. Lin, Y.; Wang, J.; Zhang, Z.-G.; Bai, H.; Li, Y.; Zhu, D.; Zhan, X. An Electron Acceptor Challenging Fullerenes for Efficient Polymer Solar Cells. *Adv. Mater.* **2015**, *27*, 1170–1174. [[CrossRef](#)]
134. Lin, Y.; He, Q.; Zhao, F.; Huo, L.; Mai, J.; Lu, X.; Su, C.-J.; Li, T.; Wang, J.; Zhu, J.; et al. A Facile Planar Fused-Ring Electron Acceptor for As-Cast Polymer Solar Cells with 8.71% Efficiency. *J. Am. Chem. Soc.* **2016**, *138*, 2973–2976. [[CrossRef](#)]
135. Zhao, W.; Li, S.; Yao, H.; Zhang, S.; Zhang, Y.; Yang, B.; Hou, J. Molecular Optimization Enables over 13% Efficiency in Organic Solar Cells. *J. Am. Chem. Soc.* **2017**, *139*, 7148–7151. [[CrossRef](#)] [[PubMed](#)]
136. Zhang, H.; Yao, H.; Hou, J.; Zhu, J.; Zhang, J.; Li, W.; Yu, R.; Gao, B.; Zhang, S.; Hou, J. Over 14% Efficiency in Organic Solar Cells Enabled by Chlorinated Nonfullerene Small-Molecule Acceptors. *Adv. Mater.* **2018**, *30*, 1800613. [[CrossRef](#)] [[PubMed](#)]
137. Li, X.; Huang, G.; Zheng, N.; Li, Y.; Kang, X.; Qiao, S.; Jiang, H.; Chen, W.; Yang, R. High-Efficiency Polymer Solar Cells Over 13.9% With a High  $V_{OC}$  Beyond 1.0 V by Synergistic Effect of Fluorine and Sulfur. *Sol. RRL* **2019**, *3*, 1900005. [[CrossRef](#)]
138. Jiao, C.; Pang, C.; An, Q. Nonfullerene Organic Photovoltaic Cells Exhibiting 13.76% Efficiency by Employing Upside-down Solvent Vapor Annealing. *Int. J. Energy Res.* **2019**, *43*, 8716–8724. [[CrossRef](#)]
139. Cui, Y.; Yao, H.; Hong, L.; Zhang, T.; Xu, Y.; Xian, K.; Gao, B.; Qin, J.; Zhang, J.; Wei, Z.; et al. Achieving Over 15% Efficiency in Organic Photovoltaic Cells via Copolymer Design. *Adv. Mater.* **2019**, *31*, 1808356. [[CrossRef](#)]
140. Zhang, Z.; Guang, S.; Yu, J.; Wang, H.; Cao, J.; Du, F.; Wang, X.; Tang, W. Over 15.5% Efficiency Organic Solar Cells with Triple Sidechain Engineered ITIC. *Sci. Bull.* **2020**, *65*, 1533–1536. [[CrossRef](#)]
141. Yuan, J.; Zhang, Y.; Zhou, L.; Zhang, C.; Lau, T.; Zhang, G.; Lu, X.; Yip, H.; So, S.K.; Beaupré, S.; et al. Fused Benzothiadiazole: A Building Block for N-Type Organic Acceptor to Achieve High-Performance Organic Solar Cells. *Adv. Mater.* **2019**, *31*, 1807577. [[CrossRef](#)]
142. Li, G.; Zhang, X.; Jones, L.O.; Alzola, J.M.; Mukherjee, S.; Feng, L.; Zhu, W.; Stern, C.L.; Huang, W.; Yu, J.; et al. Systematic Merging of Nonfullerene Acceptor  $\pi$ -Extension and Tetrafluorination Strategies Affords Polymer Solar Cells with >16% Efficiency. *J. Am. Chem. Soc.* **2021**, *143*, 6123–6139. [[CrossRef](#)] [[PubMed](#)]

143. Li, D.; Sun, C.; Yan, T.; Yuan, J.; Zou, Y. Asymmetric Non-Fullerene Small-Molecule Acceptors toward High-Performance Organic Solar Cells. *ACS Cent. Sci.* **2021**, *7*, 1787–1797. [[CrossRef](#)] [[PubMed](#)]
144. Kan, B.; Chen, X.; Gao, K.; Zhang, M.; Lin, F.; Peng, X.; Liu, F.; Jen, A.K.-Y. Asymmetrical Side-Chain Engineering of Small-Molecule Acceptors Enable High-Performance Nonfullerene Organic Solar Cells. *Nano Energy* **2020**, *67*, 104209. [[CrossRef](#)]
145. Chen, X.; Kan, B.; Kan, Y.; Zhang, M.; Jo, S.B.; Gao, K.; Lin, F.; Liu, F.; Peng, X.; Cao, Y.; et al. As-Cast Ternary Organic Solar Cells Based on an Asymmetric Side-Chains Featured Acceptor with Reduced Voltage Loss and 14.0% Efficiency. *Adv. Funct. Mater.* **2020**, *30*, 1909535. [[CrossRef](#)]
146. Xia, T.; Li, C.; Ryu, H.S.; Sun, X.; Woo, H.Y.; Sun, Y. Asymmetrically Alkyl-Substituted Wide-Bandgap Nonfullerene Acceptor for Organic Solar Cells. *Sol. RRL* **2020**, *4*, 2000061. [[CrossRef](#)]
147. Fu, Y.; Lee, T.H.; Chin, Y.-C.; Pacalaj, R.A.; Labanti, C.; Park, S.Y.; Dong, Y.; Cho, H.W.; Kim, J.Y.; Minami, D.; et al. Molecular Orientation-Dependent Energetic Shifts in Solution-Processed Non-Fullerene Acceptors and Their Impact on Organic Photovoltaic Performance. *Nat. Commun.* **2023**, *14*, 1870. [[CrossRef](#)]
148. Chen, S.; Feng, L.; Jia, T.; Jing, J.; Hu, Z.; Zhang, K.; Huang, F. High-Performance Polymer Solar Cells with Efficiency over 18% Enabled by Asymmetric Side Chain Engineering of Non-Fullerene Acceptors. *Sci. China Chem.* **2021**, *64*, 1192–1199. [[CrossRef](#)]
149. Luo, Z.; Gao, Y.; Lai, H.; Li, Y.; Wu, Z.; Chen, Z.; Sun, R.; Ren, J.; Zhang, C.; He, F.; et al. Asymmetric Side-Chain Substitution Enables a 3D Network Acceptor with Hydrogen Bond Assisted Crystal Packing and Enhanced Electronic Coupling for Efficient Organic Solar Cells. *Energy Environ. Sci.* **2022**, *15*, 4601–4611. [[CrossRef](#)]
150. Xiao, C.; Wang, X.; Zhong, T.; Zhou, R.; Zheng, X.; Liu, Y.; Hu, T.; Luo, Y.; Sun, F.; Xiao, B.; et al. Hybrid Cycloalkyl-Alkyl Chain-Based Symmetric/Asymmetric Acceptors with Optimized Crystal Packing and Interfacial Exciton Properties for Efficient Organic Solar Cells. *Adv. Sci.* **2023**, *10*, 2206580. [[CrossRef](#)]
151. Li, C.; Zhou, J.; Song, J.; Xu, J.; Zhang, H.; Zhang, X.; Guo, J.; Zhu, L.; Wei, D.; Han, G.; et al. Non-Fullerene Acceptors with Branched Side Chains and Improved Molecular Packing to Exceed 18% Efficiency in Organic Solar Cells. *Nat. Energy* **2021**, *6*, 605–613. [[CrossRef](#)]
152. Ryu, H.S.; Lee, H.G.; Shin, S.-C.; Park, J.; Kim, S.H.; Kim, E.J.; Shin, T.J.; Shim, J.W.; Kim, B.J.; Woo, H.Y. Terminal Alkyl Substitution in an A–D–A-Type Nonfullerene Acceptor: Simultaneous Improvements in the Open-Circuit Voltage and Short-Circuit Current for Efficient Indoor Power Generation. *J. Mater. Chem. A* **2020**, *8*, 23894–23905. [[CrossRef](#)]
153. Li, Y.; Zheng, N.; Yu, L.; Wen, S.; Gao, C.; Sun, M.; Yang, R. A Simple Phenyl Group Introduced at the Tail of Alkyl Side Chains of Small Molecular Acceptors: New Strategy to Balance the Crystallinity of Acceptors and Miscibility of Bulk Heterojunction Enabling Highly Efficient Organic Solar Cells. *Adv. Mater.* **2019**, *31*, 1807832. [[CrossRef](#)] [[PubMed](#)]
154. Mahmood, A.; Wang, J.-L. Machine Learning for High Performance Organic Solar Cells: Current Scenario and Future Prospects. *Energy Environ. Sci.* **2021**, *14*, 90–105. [[CrossRef](#)]
155. Zhang, Q.; Zheng, Y.J.; Sun, W.; Ou, Z.; Odunmbaku, O.; Li, M.; Chen, S.; Zhou, Y.; Li, J.; Qin, B.; et al. High-Efficiency Non-Fullerene Acceptors Developed by Machine Learning and Quantum Chemistry. *Adv. Sci.* **2022**, *9*, 2104742. [[CrossRef](#)] [[PubMed](#)]
156. Li, J.; Ballmer, S.G.; Gillis, E.P.; Fujii, S.; Schmidt, M.J.; Palazzolo, A.M.E.; Lehmann, J.W.; Morehouse, G.F.; Burke, M.D. Synthesis of Many Different Types of Organic Small Molecules Using One Automated Process. *Science* **2015**, *347*, 1221–1226. [[CrossRef](#)]
157. Trobe, M.; Burke, M.D. The Molecular Industrial Revolution: Automated Synthesis of Small Molecules. *Angew. Chem. Int. Ed.* **2018**, *57*, 4192–4214. [[CrossRef](#)]
158. Li, S.; Jira, E.R.; Angello, N.H.; Li, J.; Yu, H.; Moore, J.S.; Diao, Y.; Burke, M.D.; Schroeder, C.M. Using Automated Synthesis to Understand the Role of Side Chains on Molecular Charge Transport. *Nat. Commun.* **2022**, *13*, 2102. [[CrossRef](#)]
159. Bhat, V.; Callaway, C.P.; Risko, C. Computational Approaches for Organic Semiconductors: From Chemical and Physical Understanding to Predicting New Materials. *Chem. Rev.* **2023**, *123*, 7498–7547. [[CrossRef](#)]
160. Monteiro-de-Castro, G.; Borges, I. A Hammett’s Analysis of the Substituent Effect in Functionalized Diketopyrrolopyrrole (DPP) Systems: Optoelectronic Properties and Intramolecular Charge Transfer Effects. *J. Comput. Chem.* **2023**, *44*, 2256–2273. [[CrossRef](#)]
161. Kranthiraja, K.; Saeki, A. Machine Learning-Assisted Polymer Design for Improving the Performance of Non-Fullerene Organic Solar Cells. *ACS Appl. Mater. Interfaces* **2022**, *14*, 28936–28944. [[CrossRef](#)]
162. Miyake, Y.; Kranthiraja, K.; Ishiwari, F.; Saeki, A. Improved Predictions of Organic Photovoltaic Performance through Machine Learning Models Empowered by Artificially Generated Failure Data. *Chem. Mater.* **2022**, *34*, 6912–6920. [[CrossRef](#)]
163. Miyake, Y.; Saeki, A. Machine Learning-Assisted Development of Organic Solar Cell Materials: Issues, Analyses, and Outlooks. *J. Phys. Chem. Lett.* **2021**, *12*, 12391–12401. [[CrossRef](#)] [[PubMed](#)]
164. Feng, J.; Wang, H.; Ji, Y.; Li, Y. Molecular Design and Performance Improvement in Organic Solar Cells Guided by High-Throughput Screening and Machine Learning. *Nano Sel.* **2021**, *2*, 1629–1641. [[CrossRef](#)]
165. Park, S.; Kim, T.; Yoon, S.; Koh, C.W.; Woo, H.Y.; Son, H.J. Progress in Materials, Solution Processes, and Long-Term Stability for Large-Area Organic Photovoltaics. *Adv. Mater.* **2020**, *32*, 2002217. [[CrossRef](#)]

**Disclaimer/Publisher’s Note:** The statements, opinions and data contained in all publications are solely those of the individual author(s) and contributor(s) and not of MDPI and/or the editor(s). MDPI and/or the editor(s) disclaim responsibility for any injury to people or property resulting from any ideas, methods, instructions or products referred to in the content.